

Carbon Nanotube-Based Composites Synthesized Using Porous Aluminum Oxide

Alla Vorobjova^{*1}, Vladimir Labunov², Boris Shulitski³

¹⁻³Belarusian State University of Informatics and Radioelectronics,
P. Brovka St. 6, Minsk, 220013, Belarus

¹vorobjova@bsuir.by

I. INTRODUCTION

Porous anodic aluminum oxide (AAO) possesses uniform porous structure with hexagonal packing of cylindrical channels and narrow distribution of a pore sizes. The combination of unique porous structure with high temperature, mechanical and chemical stability does AAO films attractive to synthesis of various nanomaterials including carbon nanotube-based composites [1-5].

Devices on the basis of carbon nanotube (CNT) were not used extensively up to date [6]. That is connected with a problem of receiving the reliable, corresponding to the sizes and properties of CNT, electrode systems [7]. As a rule, usually represented CNT-devices contain other elements of the scheme, including electrodes, of the micron size. In devices on the base of CNT-array, electrodes can have the sizes, usual for microelements.

Arrays of carbon nanotubes (CNTs) embedded in porous anodic aluminum oxide are of essential interest as active elements in field emission cathodes [8-11], chemical and biological sensors [12-14]. "Nanovials" manufactured from the resulting composite can be easily filled, for example, with ferromagnetic materials. They are well dispersed in water and ethyl alcohol and can be used in medicine for drug delivery in vivo [15]. Nanotubes synthesized in the AAO pores possess increased adsorption properties when compared with the known carbon material, such as activated carbon, individual single- and multi-wall CNTs and can be used for the creation of hydrogen storage containers [16]. Generally for receiving vertically aliened CNT array in porous AAO chemical vapor deposition (CVD) or microwave plasma enhanced chemical vapor deposition (PECVD) methods are offered [17-19].

According to different publications, aligned CNTs can be synthesized in porous AAO with [20, 21] and without catalysts [22, 23]. In general, a localized catalyst (Ni, Fe, Co) electrochemically deposited into AAO pores is used for the CNT synthesis over a thin-film AAO/substrate (dielectric or silicon). If the AAO films with through pores (membranes) are used, the synthesis is performed with volatile catalysts, since the electrochemical metal deposition into the pores with high aspect ratio represents a complex technological task. However, the results presented in different publications are contradictory and do not yield an unambiguous idea of the catalyst influence and CNT growth mechanism in the porous AAO.

In this chapter processes of carbon nanotube-based composites formation with use of porous AAO are presented. We considered the synthesis of aligned carbon nanotubes in the AAO pores by CVD method with both types of catalysts (localized and injected) and both types of AAO-template – membrane and thin film AAO.

Aligned, highly uniform multiwall carbon nanotubes (MWCNT) in a porous AAO membrane were grown by the injection CVD. The effectiveness of MWCNT formation was studied with various synthesis parameters. It was found that high catalyst (ferrocene) concentrations led to formation of a thick layer of MWCNT arrays on top surface of AAO membranes, which led to decrease of the pores filling with nanotubes. It was shown that the growth mechanism of the nanotubes in the AAO pores by this method was not connected with the traditionally used transition metal catalysts, no matter whether they were in a deposited (localized catalyst) or volatile (injected catalyst) state. The pre-annealing process in air atmosphere inhibited the nanotubes formation in the AAO pores. We speculate that the formation of MWCNTs in the AAO pores is governed by the pore structure reconstruction (water desorption, phase transformation) during the high-temperature (870 °C) CVD process, though this phenomenon needs further investigation.

The optimal conditions for the pores filling with nanotubes were determined. The effect of CVD synthesis conditions, as well the role of localized catalyst on the CNT nucleation and growth were studied.

It is known, single wall carbon nanotube (SWCNT) and small-diameter MWCNTs synthesis from customized templates

or catalysts is more difficult because of their relatively high activation energy in comparison to typical MWCNTs [24]. Nucleation of such CNTs requires catalyst particles of smaller diameters (about a few nanometers). This size is not easily achieved when incorporation a catalyst within an every pore of a template.

We present a process for obtaining individual vertical CNT using catalyst nanoparticles (NPs) embedded within the pores of a thin porous anodic alumina and compare it with synthesis of MWCNT in AAO without catalyst. The initial film structure consisted of an electrode Ti layer, and a basic Al layer, deposited on a Si wafer. The Al layer was anodized to create a vertically oriented pore template. The catalyst NPs of Ni with dimensions 15 ± 5 nm were formed using electrochemical deposition on an alternating current (*ac* electrochemical deposition). CNTs were synthesized from the catalyst NPs by high-temperature CVD.

These self-aligned CNTs differ from previously reported CNTs in thin AAO [24-26] as they have a potential density of $128 \text{ CNTs}/\mu\text{m}^2$ with a CNT-CNT spacing of 110 ± 5 nm. Dawn and top contacts can be produced using electrochemical and physical vapor deposition, respectively. The length of the CNTs is controlled using different height AAO with a variability of ± 15 nm. The resulting nanostructure is expected to form the basis for development of vertically oriented CNT-based electronics and sensors.

II. SPECIFIC FEATURES OF THE CARBON NANOTUBES NUCLEATION AND GROWTH IN THE POROUS ALUMINA MEMBRANE

A. Experimental

1) Synthesis of the AAO Template

The specially prepared porous AAO membranes consist of a self-ordered array of closely packed hexagonal cells containing cylindrical pores with high degree of homogeneity. Samples of 99.95% aluminum foil with a thickness of 100 ± 5 μm and a size of 3×4 cm were used as the initial material for the manufacture of porous AAO templates. Before anodization, the samples were chemically polished in a mixture of orthophosphoric and nitric acids in a proportion of 8:1 at a solution temperature of 80 ± 2 °C for 1 min. The foil thickness after polishing was 90 ± 5 μm . Then the samples were placed into distilled water (40 °C) with subsequent washing in running distilled water and drying at $90\text{--}95$ °C in an oven.

The porous anodization of foil samples was performed with a two-stage method [27] in a 4% water solution of oxalic acid. At the first stage, porous AAO with a thickness of about 50 μm was formed in the high-voltage regime [28]. Then the formed AAO was chemically removed in the selective etchant (35 ml/l of 85% H_3PO_4 + 20 g/l of CrO_3) at a temperature of 80 ± 2 °C. The second stage of anodization was performed until the aluminum foil was completely oxidized. To provide the electric regime in anodization, the stabilized analog power supply TEC 5818 was used. The forming voltage was established by scanning with a constant rate of 0.5 V/s. The electrolyte temperature (10 °C) was kept constant with a precision of ± 2.0 °C. The membranes obtained in this regime contained pores with a diameter of 50–60 nm. The membrane's thickness was 42 μm with a porous structure having aspect ratio of about 840.

After anodization, the AAO pore walls were chemically polished in a 4% water solution of H_3PO_4 at room temperature for 40 min; this resulted in a pore expansion and etching of the barrier oxide layer on the pore bottom. This procedure reduces the degree of roughness of the pore inner surface too, which is important for the CNT deposition. As a result, an AAO template with vertically aligned through pores (membrane) was obtained. After polishing, the pore diameter increased to 80–90 nm. Then, by means of magnetron sputtering one side of the porous AAO membrane was covered with a nickel film with a thickness of 30 nm (localized catalyst). These AAO membranes were subsequently subjected to the CVD process with injected catalyst.

Theoretically, for this method of vacuum metal sputtering onto porous matrices, metal atoms penetrate to a certain pore depth depending on the pore diameter, which does not exceed the double pore radius. If AAO templates with an aspect ratio larger than 500 are used, at the moment that the pore is closed by deposited metal, the metal penetration depth into the pores is much smaller than the pore length and is approximately a factor of 3 smaller than the doubled pore radius [29].

2) Synthesis of CNTs

CNTs were synthesized using injection CVD method by means of a high-temperature pyrolysis of liquid hydrocarbon (xylene [C_8H_{10}]) mixed with the volatile catalyst source (ferrocene [$\text{Fe}(\text{C}_5\text{H}_5)_2$]). This process was performed at atmospheric pressure in an Ar/NH_3 flow. Ammonia addition was supposed to facilitate the catalytic activity of Ni particles formed from the sputtered film at the high temperature synthesis conditions. The ferrocene concentration in xylene was 0.1–10(wt.%) , the injection rate of the reaction mixture into the reactor zone was 1 ml/min, the temperature was 870 °C, the argon flow rate was 100 cm^3/min , and the flow rate of NH_3 was 10 cm^3/min . The synthesis duration was 1–10 min.

The experimental results for five CNT synthesis regimes (modes) are: in regime I, 1% feeding solution was injected for 1–10 min; in regime II, these parameters were 10% and 1 min; in regime III, 0.1% and 1–10 min, and in regime IV, V, 1% and 1 min respectively. In regime IV, 1% feeding solution was injected for 1 min but without NH_3 supply. Thus, regime I differs from regime II and III only by the used feeding solution concentration, and regime I differs from regime IV and V by

the NH_3 addition to the carrier gas flow, and from regime V by the stationary catalyst addition to the bottom of pores. The specific features of CNT synthesis modes are presented in Table 1.

TABLE 1 SPECIFIC FEATURE OF CNT SYNTHESIS MODES

Regime mode	I	II	III	IV	V
Ferrocene concentration, %	1	10	0.1	1	1
Duration of synthesise, min	1-10	1	1-10	1	1
NH_3 availability	yes	yes	yes	no	yes
Stationary catalyst	Ni	Ni	Ni	Ni	no

3) Characterization Techniques

The morphology and structure of the samples were investigated by scanning electron microscopy, SEM (Phillips XL30 S FEG and Hitachi S-4800); transmission electron microscopy, TEM (Phillips CM-30); Raman spectroscopy (LabRam Aramis Raman Spectrometer, Horiba Scientific, laser wavelength $\lambda=532$ nm) and Raman scattering spectroscopy (a solid state Nicolet Spectrometer NECSUS 720 laser with the wavelength $\lambda=1064$ nm and a power of 0.1–3 W); Auger electron spectroscopy (EAS spectrometer PHI 660); X-ray photoelectron spectroscopy (XRPES spectrometer ES 2401 with a hemispherical electron analyzer) and IR spectroscopy (Perkin-Elmer Spectrum One).

B. Results and Discussion

1) The Effect of CVD Regime

It was observed that the AAO membranes after the CNT synthesis process using the feeding solution concentrations of 1-10% appeared to be covered with a thick layer of entangled CNT arrays. Fig. 1 shows SEM images of the samples obtained in regime I: as-synthesized (Fig. 1(A)) and after mechanical cleaning of the AAO surface from the CNT crust on top (Fig. 1(B)).

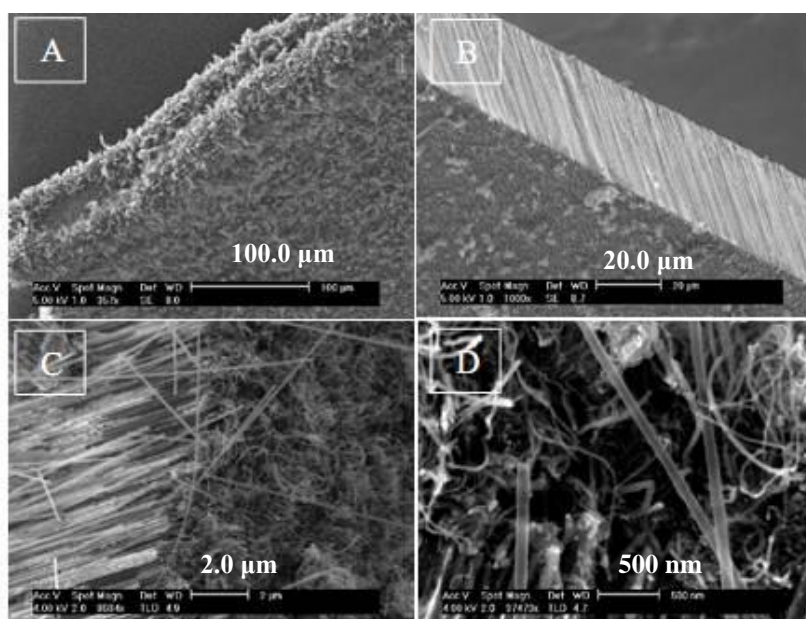


Fig. 1 SEM images of the AAO membranes after CNT synthesis in regime I, 10min (A) as-synthesized; (B) after mechanical cleaning of the top CNT crust; (C, D) magnified views of the AAO cross section showing the nanotubes grown on top and in the pores

CNTs formed on the AAO surface begin to grow actively only if the ferrocene concentration increases to 1.0% and higher. These CNTs produced on the surface of the sample have significantly smaller diameters (from 10 to 20 nm) than that grown inside AAO since it is not controlled by the pore size of the AAO membrane (Fig. 1 (C, D) and Fig. 2 (C, D)). The difference observed in the carbon material formed on the sample surface and in the AAO pores is governed by the peculiarities of their formation mechanism.

It is seen in Fig. 2 (A, B) that the aligned nanotubes repeating the pore shape were formed in the AAO membrane. It is noteworthy that the diameter of the pores appeared to be slightly increased to 70-100 nm (regime III) or 100-130 nm (regime I), depending on the initial diameter of pore after the CVD process. The nanotubes were open-ended, the internal diameter was about 50–70 nm, and they did not contain visible structural defects.

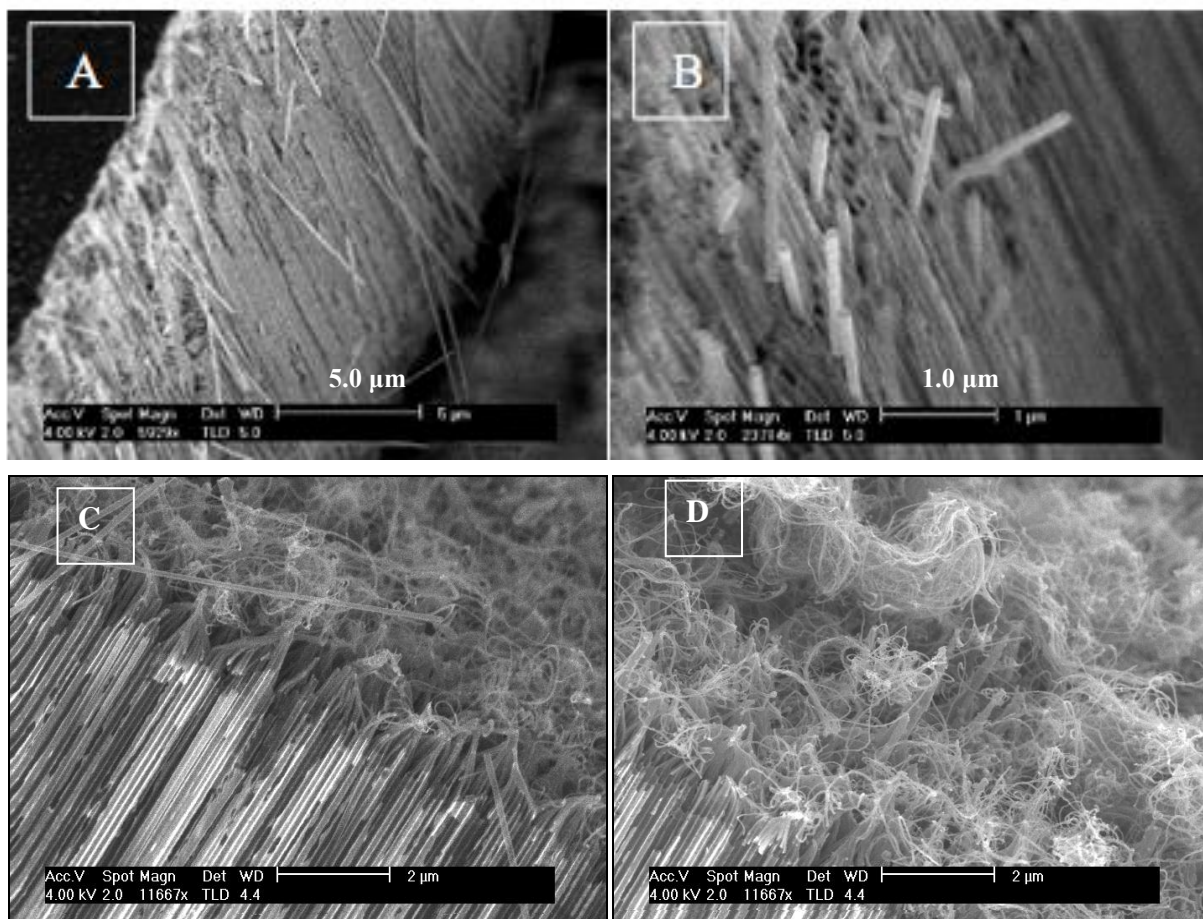


Fig. 2 SEM images of the AAO cross section (A, B) and surface (C, D) showing the nanotubes grown in the pores and on the surface in regime I, 6min

For comparison, SEM images of the sample obtained in regime II are presented in Fig. 3. This regime differs from regime I only by a higher feeding solution concentration. It is noticeable that there were fewer nanotubes filling the pores (Fig. 3(A)) which may be caused by a very thick CNT crust layer grown on top of the membrane (Fig. 3(B)) which hindered the diffusion of the feedstock into the pores thus preventing the nanotube formation.

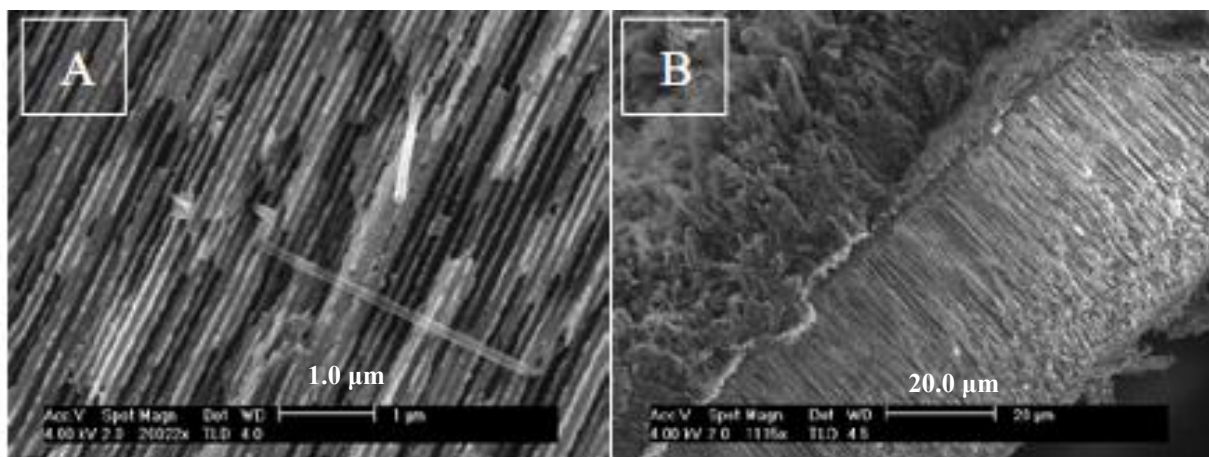


Fig. 3 SEM images of AAO membranes after CNT synthesis in regime II. (A) - A few nanotubes protruding from the AAO pores; (B) - general view of the sample with a 30 μm CNT crust layer on top

It can be seen from Fig. 2 that aligned tubes with the same configuration as in regime I were formed in AAO pores, but disaligned entangled CNTs with a significantly smaller diameter were produced on the sample surface. Obviously the growth of these CNTs is not in anyway connected with the pores in the template and tubes formed in these pores. The difference in the carbon material formed on the sample surface is due to the different ferrocene concentration in the reaction mixture. CNTs formed on the AAO surface begin to grow actively only if the ferrocene concentration increases to 1.0% (all regimes except III). Fine iron particles of small diameters formed in ferrocene pyrolysis are probably in the state of

suspension and chaotically distributed in the reaction zone. If the ferrocene concentration sufficiently increases, iron particles are adsorbed on the AAO surface and become centers of formation of common carbon nanotubes, which are entangled in an arbitrary way above the template surface in the course of growth, forming “clews”. The diameter of such tubes (from 10 to 20 nm) is much smaller than the diameter of tubes in the AAO template; i.e., it is not connected with the pore diameter in the template.

In order to eliminate the formation of the CNT crust layer, the synthesis in regime III was conducted with the reduced concentration of ferrocene in the feeding solution but with different deposition time (Fig. 4). As a result, the nanotubes were formed in almost all the pores of AAO.

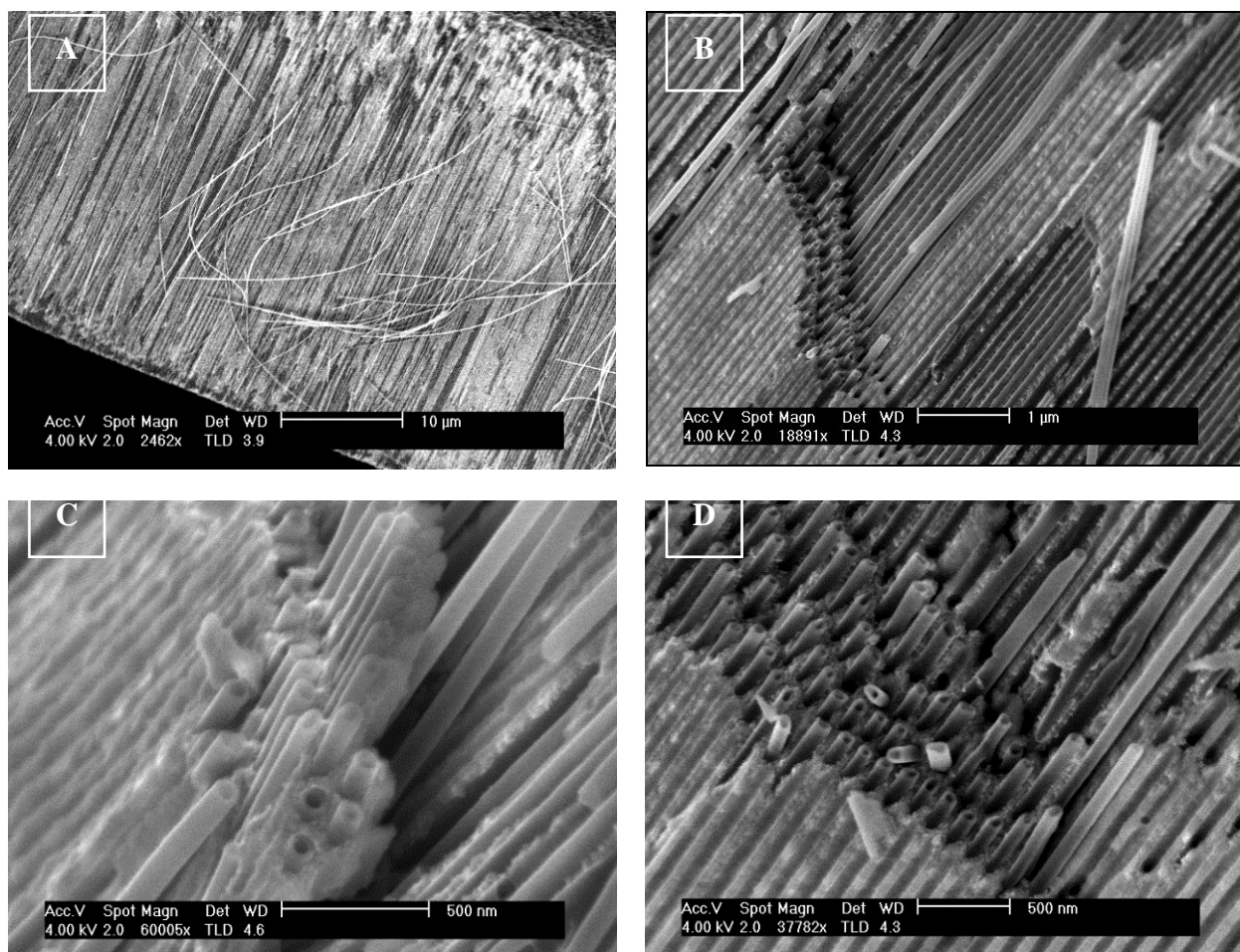


Fig. 4 SEM images of the AAO membranes after CNT synthesis in regime III, 3 min (A), 6 min (B-D)

After synthesis MWCNT it was carried out chemical etching of a membrane in fluoric acid and 10% water solution of NaOH. Neither oxide nor tubes practically do collapse at such processing. Only after ionic cleaning in the atmosphere of argon (energy of ions 3keV) partial etching of oxide was observed. Tubes thus remained absolutely safe and sound. It can be seen from Fig. 4(B, D) that, as a result of ion cleaning, disorganized carbon were completely removed from the surface and the AAO was partially etched. Fig. 4(C) is SEM photo of the same sample after combine processing (chemical etching and then ion bombardment).

Furthermore, the effect of ammonia was investigated. For this purpose, we repeated the regime I, but excluded NH_3 from the gas flow (regime IV). It was revealed that the nanotubes having much thinner walls were formed in the AAO pores (Fig. 5(A) and the inset).

Based on the results of SEM investigation presented it can be concluded that in the samples obtained in different synthesis regimes, the aligned carbon nanotubes repeating the pore shape are formed within a porous AAO membrane. If the ferrocene concentration increases by up to 1.0% and higher, an entangled CNT layer having much smaller nanotube diameters is formed on the AAO surface. The catalyst precursor concentration used for the synthesis process increases the thickness of CNT layer on top of AAO increases, preventing the diffusion of carbon feedstock into the pores, and thus restricting the nanotubes growth inside the AAO pores. The addition of NH_3 into the gas flow promotes the thickening of the nanotube walls. The conditions of regime III are considered as optimal for the nanotube formation in the AAO pores.

However, the role of Ni as catalyst was not evidenced by SEM studies and will be discussed later.

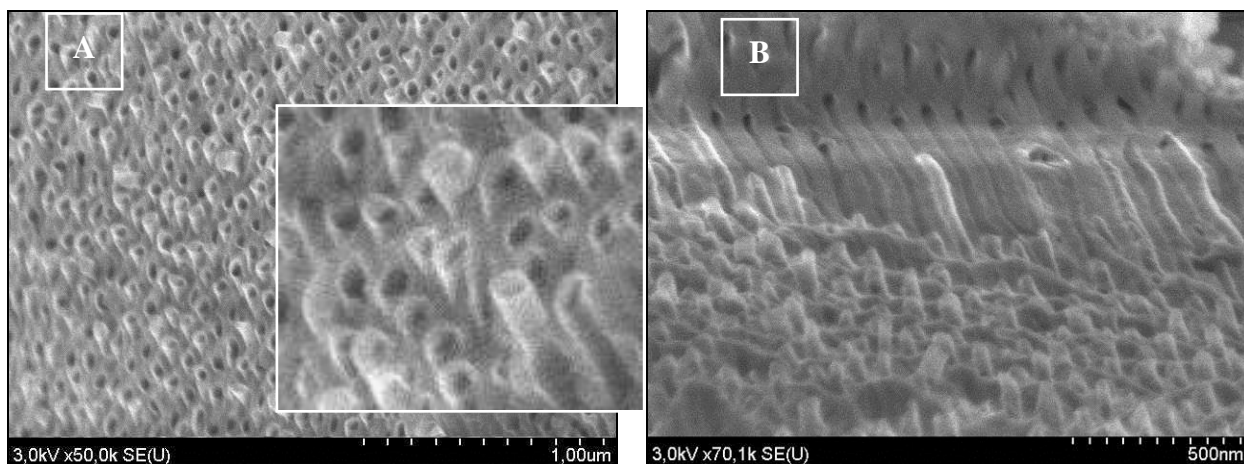


Fig. 5 SEM top view (A) and cross-section view (B) of the AAO membrane after CNT synthesis in regime III, 5 min

2) The Structural Properties of Nanotubes

For TEM analysis, the samples were first mechanically ground, sonicated in isopropyl alcohol, and then put onto a copper grid. The difference in the geometric size and shape of the nanotubes formed inside the membrane and on its surface is clearly illustrated in Fig. 6, where Fig. 6(A) shows TEM images of the nanotubes formed in the pores of AAO in regime IV. They have relatively large diameters of about 130 nm and look brittle. During TEM analysis, lots of damaged and unzipped nanotubes rather like graphene flakes (pointed with an arrow in Fig. 6(A)) were found. In Fig. 6(B) along with the nanotubes grown in the AAO pores (1) the carbon nanotubes (2) grown on the surface of AAO membrane are indicated. This kind of nanotubes has diameters of about 20-60 nm and even has catalyst nanoparticles inclusions in their channels (indicated with arrows in Fig. 6(B)).

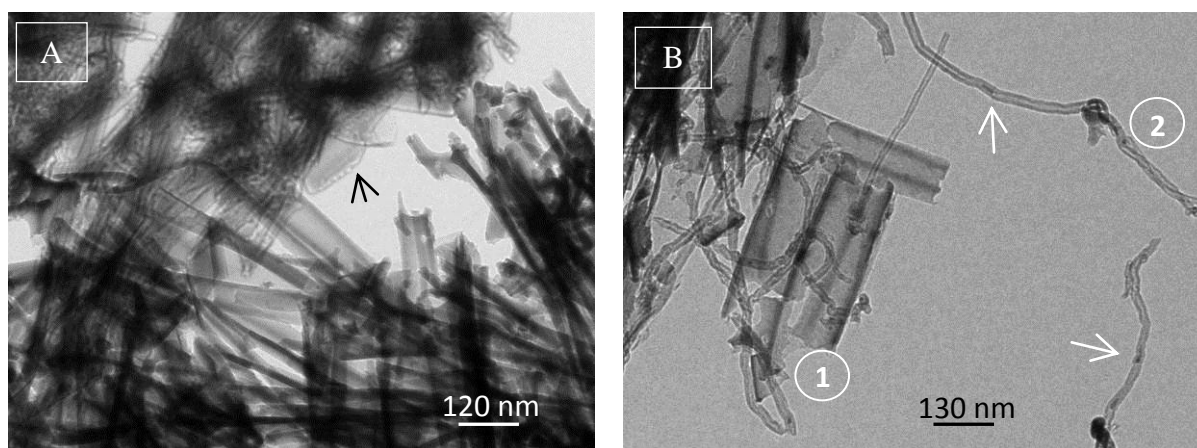


Fig. 6 TEM images of the nanotubes of two types: (A) nanotubes grown inside the AAO pores; (B) classical CNTs grown on the AAO surface (1) and the nanotubes grown inside the AAO pores (2). Catalyst nanoparticles are indicated with arrows

This is the evidence that these CNTs are classical for they were grown via extrusion of graphite fraction from carbide phase (most likely, iron carbide from ferrocene decomposition) of catalytic nanoparticles during CVD [30]. The growth mechanism of the tubes formed in the pores will be discussed later.

For the investigation of the structure of the nanotubes formed in the AAO pores, the samples were studied by Raman spectroscopy. Fig. 7(A) shows the typical Raman spectra of the pristine AAO and the AAO sample after the CNT synthesis (regime I) followed by surface cleaning. Raman spectrum exhibited two distinct peaks at 1590 and 1355 cm^{-1} which are the feature of graphitic materials. The band at 1550-1605 cm^{-1} (G band) is attributed to E_{2g} symmetry in-plane optical mode associated with the stretching of all C=C pairs, while the band near 1350 cm^{-1} (D band) is physically related to the in-plane A_{1g} symmetry breathing mode of the C hexagon which intensifies and broadens when the amount of structural defects increases. The ratio ID/IG obtained after the background subtraction and fitting with two Gaussians is 0.83, which is lower than that obtained for the nanotubes grown in AAO using C_2H_2 decomposition [31] yet still quite high. This ratio may indicate a semicrystalline carbon structure with some plane defects and lattice edges. Unfortunately, the way of stacking

order of graphitic planes cannot be estimated from this data as the G' band is out of the measured range, but most probably it is similar to turbostratic graphite [32].

The elemental composition on a surface and in the volume of the samples synthesized in a regime III was investigated by the Auger spectroscopy with profiling along the membrane depth after the mechanical cleaning of its surface. The uniform distribution of basic elements – Al, O, and C along the sample depth was established, with relative atomic concentrations of 29, 54 and 18%, respectively (Fig. 7(B)). Neither nickel nor iron, from the decomposed ferrocene was detected.

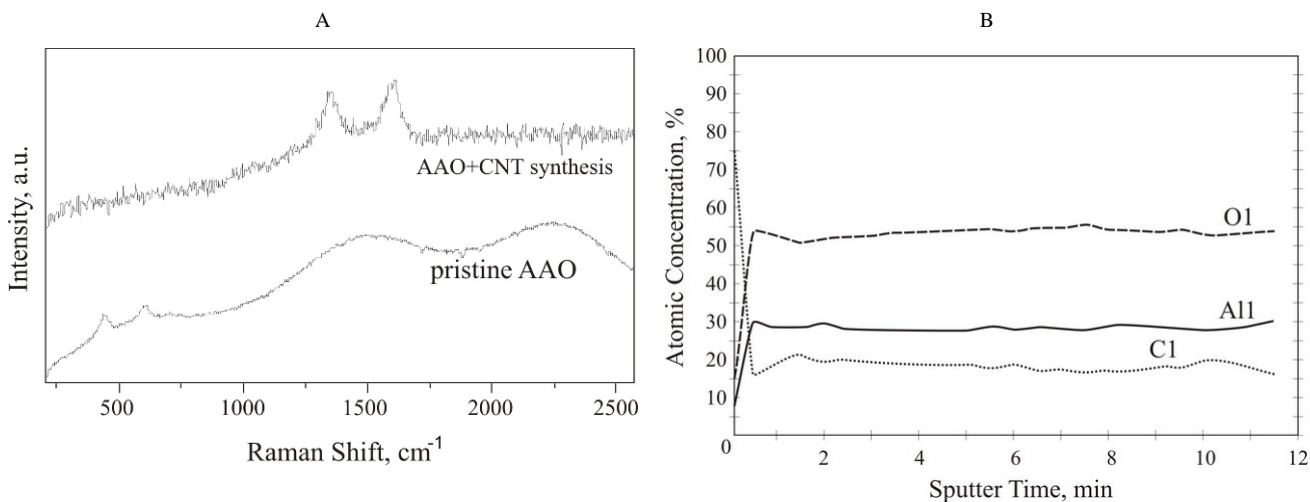


Fig. 7 Raman (A) and Auger electron (B) spectra recorded from the sample obtained in regime III (after the surface cleaning)

X-ray photoelectron spectroscopy was used to obtain information on the chemical state of elements in the volume of the AAO template with carbon tubes. Monochromatic Mg K_α emission with a power of 300 W directed 45° to the analysed surface was used for photoemission excitation. The spectra were registered in the spectrometer chamber at a residual gas pressure of no worse than 8×10^{-8} Pa. The spectra were calibrated by a peak of a 1s carbon level with a binding energy of 285.0 eV due to the photoelectron emission from carbon atoms in C–H groups. The chemical state of elements of the sample surface was estimated by shifts of energy peaks in the high resolution spectra of C 1s and Al 2p lines. Surface sputtering by a low power argon ion beam was used to change the depth of the analysis in the sample volume. The processing (decomposition into separate components) of the X-ray photoelectron spectra was performed using the method presented in [33] with background subtraction using the Sherwood algorithm.

The plain photoelectron spectra of the samples subject to the mechanical removal of the surface CNTs and partial surface sputtering by argon ions contained peaks identifying Al, O, and C atoms. Photoelectron peaks from Fe atoms were absent in plain spectra. An analysis of the high resolution spectra of these elements and a comparison with the known published data made it possible to formulate a qualitative conclusion about the chemical state of elements in the material of the carbon-tube walls embedded in AAO pores.

Fig. 8 shows the photoelectron spectra of island C 1s and Al 2p levels of the sample synthesized in regime 1 and the results of their decomposition into components.

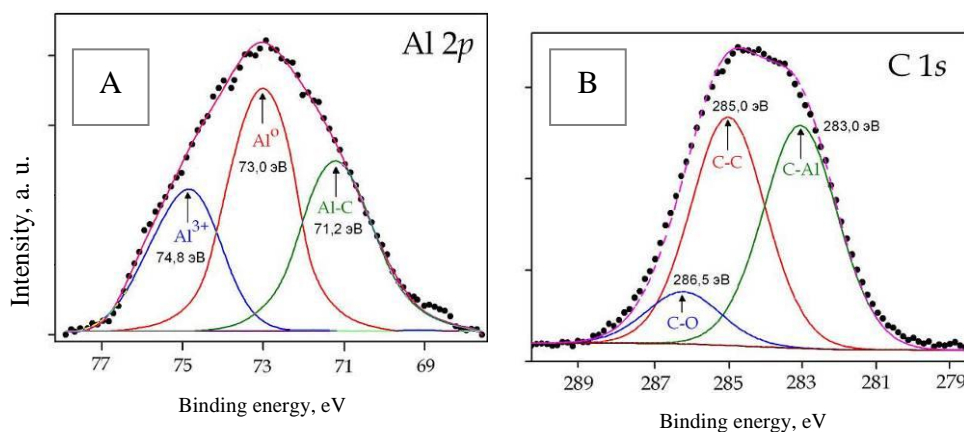


Fig. 8 X-ray photoelectron spectra of (A) island 1s level of carbon and (B) island 2p level of aluminum; the results of their decomposition for nanocomposite carbon material synthesized in regime 1 after the sputtering of ~1 μm of the sample surface by argon ions

It can be seen from Fig. 8(A) that the C 1s spectrum is complex and can be decomposed into three pronounced components in the form of symmetric peaks shifted with respect to each other with maxima at 283.0, 285.0, and 286.5 eV. The spectrum of the Al 2p level (Fig. 8(B)) can also be decomposed into three components with the binding energies $E_b = 71.2, 73.0,$ and 74.8 eV. Note that the difference in the binding energies of C 1s peaks related to the atmospheric carbon and carbon in the studied material is not large and cannot be reliably proven by X-ray photoelectron spectroscopy without varying the X-ray angle.

However, taking into account the relative intensity of the C 1s peak with $E_b = 285.0$ eV and the presence of this peak in the spectrum of the sample whose surface was sputtered in vacuum by argon ions (i.e., in conditions when the presence of the adsorbed hydrocarbons is eliminated), it can be assumed that the C 1s peak with $E_b = 285.0$ eV corresponds to the C=C bond in the synthesized carbon tubes, although the particular character of carbon hybridization (for example, sp^2 or sp^3) cannot be established based on this decomposition. Then the high-energy carbon 1s peak should be related to the photoelectrons emitted by the carbon–oxygen bond in C=O groups whose presence is determined by electrolyte anions $C_2O_4^{2-}$ in AAO film or their derivatives embedded in AAO structure upon anodization. Of greatest interest in the spectrum of the carbon 1s level is the low-energy peak with $E_b = 283.0$ eV, which is not a typical component of the C 1s spectra of AAO or graphite [34]. This additional low-energy peak can be due to the additional chemical bond between carbon atoms and atoms of another chemical element, for example, relatively more electropositive metal.

The components of expansion of the photoelectron spectrum of the Al 2p level (Fig. 8(B)) can be interpreted as follows: The first high-energy peak with $E_b = 74.8$ eV corresponds to the state of aluminum atoms with an oxidation degree of 3+, i.e., in the Al_2O_3 compound. The second Al 2p peak shifted with respect to the first one by -1.8 eV is determined by photoelectrons emitted by metallic aluminum [35]. The third low-energy Al 2p peak shifted by -3.6 eV with respect to the first Al $^{3+}$ 2p peak represents a nontypical spectrum component absent in the line of the island 2p level of aluminum in AAO film. Taking into account the fact that iron atoms were not detected in the studied samples, it can be assumed that this peak can be explained by the presence of carbon atoms chemically bound with aluminum atoms in the synthesized material. The character of this bond can be as follows: The shift of the third Al 2p peak to the low-energy part of the spectrum from the position of the Al^0 2p peak ($\Delta E = 1.8$ eV) essentially exceeds the spin-orbital splitting for the 2p level of aluminum. At the same time, a large shift of the low-energy C 1s peak from the C=C peak ($\Delta E = 2.8$ eV, Fig. 8(A)) cannot be explained by the charge flow from electropositive aluminum atoms to the electronegative carbon atoms interacting with them, which is accompanied by a weakening of the coupling of electrons populating the C 1s level. Therefore, it is most probable that the Al–C bond occurred as a result of carbide formation in AAO pores due to high-temperature paraxylene decomposition.

Taking into account the fact that the component areas in the decomposition of C 1s and Al 2p spectra are proportional to the concentrations of the corresponding structural elements in the film, it is obvious that the amount of metallic aluminum inside the film is many times larger than the amount that can be contained in common anodic aluminum oxide. It can be assumed that, during the synthesis of carbon tubes in the AAO template, processes which caused the following sequence of solid-state and chemical reactions took place: (a) there was a partial decay of oxygen bonds of aluminum in the external layer of the pore walls stimulated by the high temperature, structural, and chemical AAO rearrangement; (b) there was a reduction and melting of the produced aluminum, and (c) the partial interaction between the melt metallic aluminum and paraxylene in pores or the alloying of metallic aluminum with a carbon layer on the pore walls with the formation of carbide (methanide) took place according to the following mechanism:



An alternative possibility for carbide phase formation could occur as a result of the high-temperature interaction between aluminum oxide in pore walls and the carbon material that formed on the walls. Thus-formed carbide can be partially evaporated with decomposition into carbon and metallic aluminum; an anomalously large amount of metallic aluminum was discovered in the synthesized material by means of X-ray photoelectron spectroscopy.

Obviously, the formation of aluminum carbide in nanosized AAO pores takes place under these conditions at lower temperatures when compared to the classical ideas of high-temperature carbide forming reactions. The main reason for this is probably connected with the formation of catalytically active polycrystalline γ -oxide as a result of high-temperature processing. Facts such as the presence of embedded electrolyte anions, structural defects that formed as a result of deprotonization, the removal of bound water, and the redistribution of mechanical stress in anode film can contribute to this phenomenon. A similar effect of low-temperature carbide formation, as exemplified by iron, was considered in [36], which was devoted to the mechanoactivation of iron in liquid organic media due to the formation of the nanocrystalline structure in submicron particles and the saturation of their volume by products of destruction of the ground medium. In any case, the discovered phenomenon of aluminum carbide formation in carbon tube walls in nanosized AAO pores during CNT synthesis requires further experimental and theoretical studies.

Our results showed that important specific feature of the high-temperature synthesis of nanocomposite carbon material in AAO pores as one-dimensional reactors are due to the fact that AAO turns out to be involved in this physical and chemical process. Below we present an analysis of the possible transformations (modification) of porous AAO during its high-temperature processing.

3) Specific Features of the Nanotubes Growth

The results show that there are important specific features of the high temperature reconstruction of the AAO pores during CVD process. In our previous work the changes in the AAO chemical composition and structure after the high-temperature CVD process were studied by X-ray photoelectron spectroscopy (XPS) [36]. In-depth analysis of the core C 1s- and Al 2p-levels revealed (along with C-C, C-O and Al³⁺) the presence of Al-C and Al⁰ in the analysed sample. This indicated that AAO itself was involved in the physical and chemical process of CNT formation in its pores. The fact that the pore diameter was slightly increased after the synthesis supported this argument.

Indeed, the AAO membrane obtained with the use of oxalic acid may contain 6-10% of adsorbed water, and bound water (Al₂O₃·nH₂O, n=1-3). The former was desorbed at 110-130 °C, and the latter at 350-550 °C. This explains the enlargement of the pore diameter after the synthesis process. Moreover, during the synthesis process at temperatures up to 900 °C in the AAO pore Al was partially reduced and partially transformed into a crystalline γ-Al₂O₃ phase [38], which was accompanied by the shrinkage of its volume. Since aluminum carbides can be formed directly from aluminum oxide by reacting with carbon at significantly higher temperatures (~1800 °C), we suggest that only the released after the water desorption Al can react with carbon species from the gas phase thus forming carbide (most probably, Al₄C₃). As long as Al₄C₃ is stable at up to 1400 °C, it exists along with the polycrystalline γ-Al₂O₃ and probably C₂O₄²⁻ anions as a residual from the electrolyte solution, and can support or even take part in the formation of the nanotubes in the pores during CVD.

It is noteworthy that at similar synthesis conditions described in [37], neither Ni nor Fe was detected in the pores by XPS. Therefore, it raises the question that whether nickel particles formed on one side of AAO and iron particles from the ferrocene decomposition participate in the formation of nanotubes in the AAO pores. It is obvious though that last one catalyse the nucleation of CNT crust covering the surface of AAO membranes.

Thus, in a nanotube wall formation the role of the localized (nickel) and injected catalyst, as well as the pore reconstructions in the formation of nanotubes inside AAO remain unclear. In order to shed some light on this phenomenon we conducted additional experiments (regime V, see Table 1). The results are presented for four types of samples (see Table 2 and Fig. 9).

TABLE 2 CONDITIONS OF EXPERIMENTS FOR THE ASSESSMENT OF INFLUENCE OF THE LOCALIZED CATALYST

Description of Sample	Conditions of Experiments	Type of Sample
Al ₂ O ₃ membrane with or without Ni film	Annealing (820 °C, 5 min, N ₂ flow rate 100 cm ³ /min)	A (no CNT)
Al ₂ O ₃ membrane without Ni film	CVD in regime I after the AAO annealing in air (1000 °C, 60 min)	B (no CNT)
Al ₂ O ₃ membrane without Ni film	CVD in regime V	C, D (CNT)
Al ₂ O ₃ membrane with Ni film	CVD in regime I	E, F (CNT)

From the presented data it is visible that neither the annealing process in inert atmosphere (i.e. reproducing of the synthesis conditions but without ferrocene/xylene supply) nor the CNT synthesis using the annealed in air AAO membranes gave rise to the nanotubes formation in the pores (Fig. 9 (A, B)). On the other hand, carbon nanotubes were formed in the pores of pristine AAO no matter nickel did or did not deposit at the bottom of the pores (Fig. 9 (C-F)). These results testify to the facts that (i) a localized catalyst (Ni) does not play any role in the formation on nanotubes in the AAO pores; (ii) hydrocarbon from the gas phase penetrates into the AAO pores and is necessary for the nanotube formation; and (iii) during the annealing in air some modifications of the pore structure/composition occur, which inhibit the nanotube growth in our synthesis conditions. It is possible that γ-Al₂O₃ transforms into α-Al₂O₃ (>950 °C), which might be no longer favourable for the nanotube formation. The last assumption must be checked by conducting a more peculiar investigation. The role of Al₄C₃ and crystalline γ-Al₂O₃ in the formation of nanotubes also needs further study.

4) Analysis of Modification of Porous AAO during High-temperature CVD-processing

Our results showed that important specific features of the high-temperature synthesis of nanocomposite carbon material in AAO pores as one-dimensional reactors are due to the fact that AAO turns out to be involved in this physical and chemical process. Below we present an analysis of the possible transformations (modification) of porous AAO during its high-temperature processing.

According to various published data, the water content in the anodic aluminum oxide obtained in solutions of sulphuric and oxalic acids can reach 6–10% [38, 39]. The desorption of adsorbed water is observed at 110–130 °C. However, AAO contains not only free, but also bound water forming the compound Al₂O₃·nH₂O, where n can take values from 1 (a film thickness smaller than 16 μm) to 3 (a film thickness larger than 50 μm) [40]. The removal of bound water is observed in a temperature range of 350–550 °C. Therefore, in the case of high-temperature AAO annealing, the pore diameter can insignificantly increase.

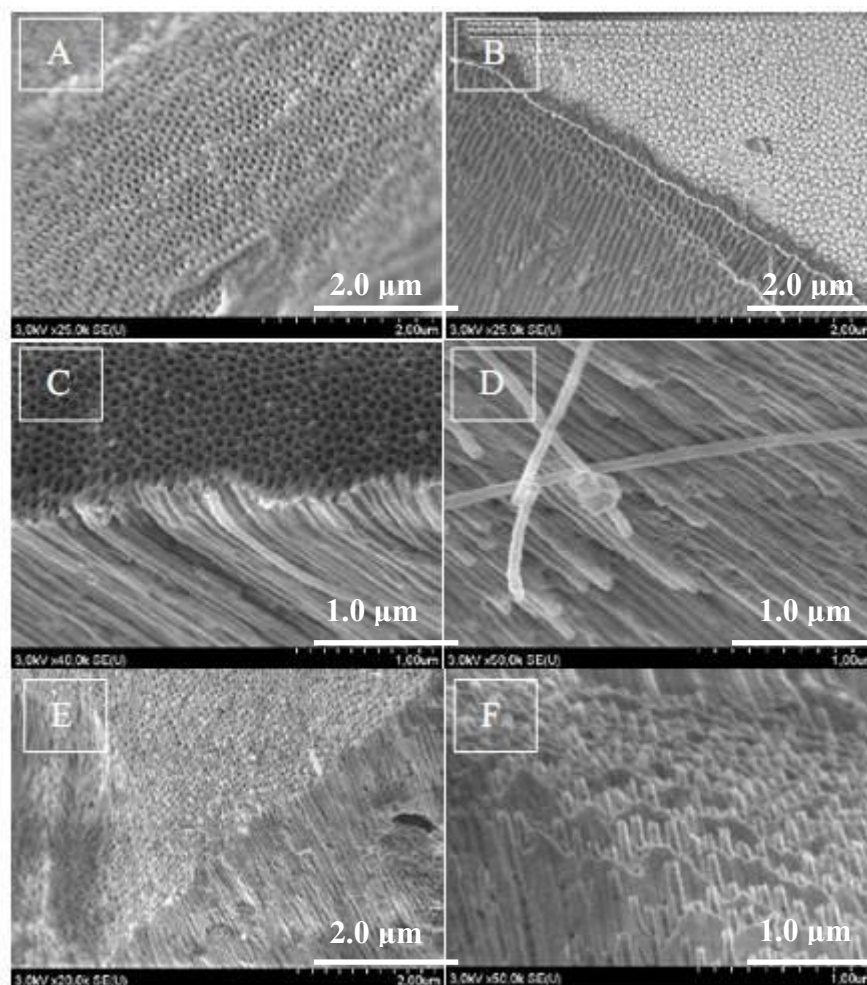


Fig. 9 Top and cross-sectional views of the samples: A – an AAO membrane annealed in N_2 atmosphere; B – an AAO membrane annealed in air followed by the CNT synthesis in regime I; C, D and E, F – CNT synthesis was carried out in regime I using AAO without and with Ni film, correspondingly. In all cases AAO was created by two-step anodizing and its thickness was about 40 μm

Transformations in AAO upon annealing are connected not only with the removal of bound water, but also with changes in the AAO structure. The changes in the AAO chemical composition and structure during annealing were studied using IR spectroscopy. It is well known that water molecules or OH groups are parts of AAO as binding elements between separate structural elements. No changes in the IR spectra were observed upon oxide heating to 100 $^{\circ}C$. When the samples were heated to 300 $^{\circ}C$, the intensity of the Al–OH absorption band (1080 cm^{-1}) essentially decreased. In the case of annealing to 500 $^{\circ}C$, AAO lost part of its bound water because of the destruction of Al–OH bridge bonds and the $Al(OH)_3$ hydrate was partially transformed into crystalline $\gamma\text{-Al}_2O_3$. This transformation was accompanied by the reduction (compression and shrinkage) of oxide in the template with the simultaneous insignificant growth of the pore diameter. It is known that the thermal compression of anodic oxide continues until 900 $^{\circ}C$. Up to 700 $^{\circ}C$ this phenomenon is reversible; at 950 $^{\circ}C$, the irreversible transformation of $\gamma\text{-Al}_2O_3$ into corundum begins. If the temperature increases further, bridge bonds of Al–OH groups are destroyed and $\alpha\text{-Al}_2O_3$ are formed. At 1000 $^{\circ}C$, all absorption bands except for 810 and 720 cm^{-1} bands corresponding to Al–O–Al bond absorption vanish.

Thus, the metastable γ modification of Al_2O_3 was formed during the synthesis of carbon tubes and the presence of this modification shifted the beginning of synthesis (the carbon interaction with the internal pore surface) toward lower temperatures. This phenomenon, known as the Hedwall effect, is connected with the increased reactivity of solids during or in the process of crystallographic transformations [41]. In our case amorphous AAO becomes polycrystalline in the course of reaction mixture heating, which is accompanied by thermal energy release. The components of the oxide lattice become more mobile upon rearrangement; this mobility can initiate chemical transformations with the participation of aluminum carbide. Moreover, system crystallization results in the sharp narrowing of the pore-size distribution; i.e., it causes additional self-ordering of the system of cell sand pores in AAO [42]. Therefore, at 850–879 $^{\circ}C$, AAO, which is amorphous before the beginning of CVD deposition, transforms into a catalytically active polycrystalline γ -oxide. The properties of such aluminum oxide to a large extent depend on the temperature growth rate: $\gamma\text{-Al}_2O_3$ is crystallized in cryptocrystalline (fine) and phanocrystalline forms. Crystallization is accompanied by the reduction of the oxide volume by 14.3% and the release of 92 kJ/mole of heat [43]. High-temperature AAO processing in the course of pyrolysis accompanied by phase

transformations (changes) in amorphous AAO, which compresses the crystalline lattice by a rather large value with the conservation of the initial structure motive, results in local stresses and possibly the additional activation of the oxide surface.

These modifications of the composition, structure, and chemical activity of the oxide template in conditions of CNT synthesis resulted in the fact that the formation and growth of carbon tubes took place simultaneously on the whole surface of the pore walls in AAO; this surface played the forming and catalytic role. At the same time, it became obvious that, for these synthesis conditions (first and foremost, the given temperature), the processes taking place on the AAO pore surface suppress the catalytic activity of nickel particles. Iron particles from ferrocene played the role of catalytic centers of the nucleation of classical CNTs not connected with the pore size on the surface of anodic oxide.

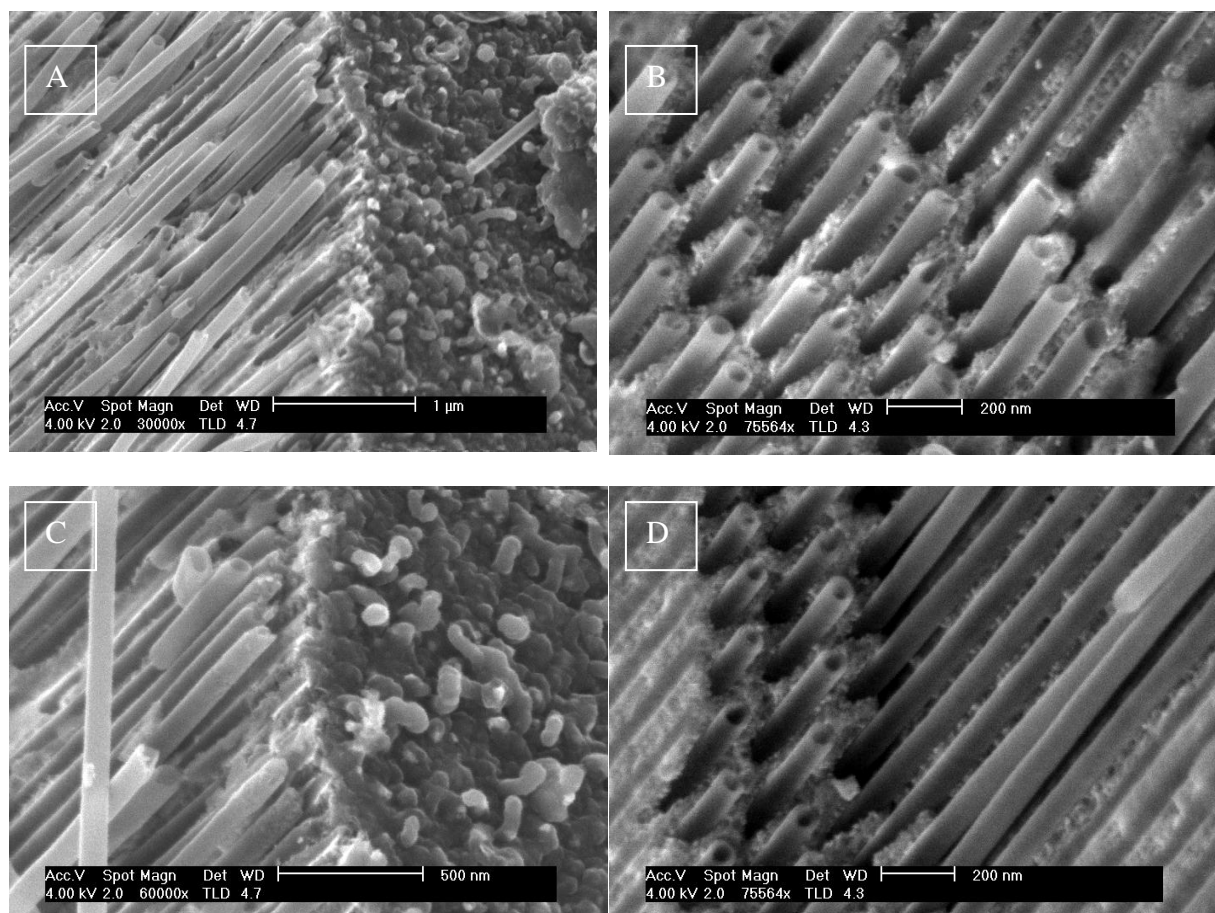


Fig. 10 Top and cross-sectional views of the different segments (fragments) of samples after CNT synthesis in regime III: A, C – before and B, D after the ion cleaning of the surface

C. Conclusions

In summary, the formation of carbon nanotubes in aluminium oxide membranes was investigated in various CVD conditions. It was found that relatively high catalyst concentrations inhibit the formation of nanotubes inside AAO, since a thick CNT carpet is formed on the AAO membrane surface, which blocks the diffusion of reagents into the pores. Optimal conditions of CVD for the nanotube formation were found. It was established that neither deposited Ni nor iron from the ferrocene decomposition catalyses the formation of the nanotubes in AAO. Moreover, after the high-temperature annealing in air, AAO no longer supports the nanotubes formation in its pore by this method. We speculate that the formation of carbon nanotubes in the AAO pores is governed by the pore structure reconstruction (such as water desorption, phase transformation) during the high-temperature CVD process.

It was demonstrated that the application of free films of porous AAO as templates in the CVD synthesis of CNTs makes it possible to concentrate reagents in a bounded nanosized space (pores), isolating them from external influence, which increases the efficiency of the spatially bounded formation processes of new substances and materials. It was established that the structural and morphological changes in porous AAO that take place in the synthesis of carbon tubes activate the surface of the pore walls, which acquire unique catalytic properties for carbon tube growth and become an important component of the system of reagents contributing to the formation of the new carbon-containing material with improved physical and chemical properties (an array of carburized carbon tubes embedded in polycrystalline aluminum oxide).

It was shown that the synthesized arrays of carbon tubes with carbidized walls possess a high homogeneity in the sizes of structural elements (see Fig. 10) with the following controlled parameters: (i) the tube diameter is from 60 to 140 nm (controlled by the aluminum anodization voltage and the time of chemical polishing of AAO pore walls), (ii) the aspect ratio is no smaller than 500 (controlled by the anodization time and determined by the AAO film thickness), and (iii) the distance between tubes in an array from 100 to 180 nm (controlled by aluminum anodization voltage).

Arrays of carbidized carbon tubes embedded in porous templates of polycrystalline γ - Al_2O_3 are of essential interest as active elements in field-emission cathodes [44-46] and chemical and biological sensors [47]. Nanotubes manufactured from the resulting composite can be easily filled, for example, with ferromagnetic materials. They are well dispersed in water and ethyl alcohol and can be used in medicine for drug delivery *in vivo*. Nanotubes synthesized using the method described above possess increased adsorption properties when compared with known carbon materials (activated coal and single-layered and multilayered CNTs) and can be used separately for the creation of hydrogen storage containers [48].

III. CARBON NANOTUBE ARRAYS SYNTHESIZED BY CVD WITHIN THIN POROUS ALUMINA TEMPLATE

A. Formation of CNT-Array on Metal Electrodes Using Thin Porous Aluminum Oxide

1) Experimental

Array of vertically aligned carbon nanotubes was formed on metal electrode system using thin porous anodic aluminum oxide as a template by CVD method. As the CVD method based on high-temperature pyrolysis of liquid hydrocarbon on a surface of the metal catalyst at a temperature of 850-900 °C, the electrode system has to be rather heat-resistant. Therefore the electrodes were formed from the thin film of Ti [49].

The experimental samples represented two-layer Ti and Al thin film compositions on 6.0×4.8 cm² ceramic or 76 mm diameter Si and Si/SiO₂ substrates. The Ti film serves as an adhesion layer for the Al film and a conductive layer for anodization and other post processing.

Polycrystalline metal films of Ti and Al were produced by electron-beam evaporation in a single vacuum cycle in the 01HЭ-7-004 (Oratoriya-9) vacuum unit. The vacuum under deposition of (300 – 500) nm thickness Ti film was 1.3×10^{-3} Pa, substrate temperature was 523 K, and deposition rate was 1.0 ± 0.2 nm/s. Al film of (2000 – 3000) nm thickness was deposited onto the cooled to 423 K substrates in 1.4×10^{-4} Pa vacuum from A-995 (0.005 % of impurities) target at 6.0 ± 0.5 nm/s rate. Film thickness and deposition rate were controlled with the quartz sensor.

The top layer of Al was anodized to the Ti layer by two-step anodizing process in 4.0 wt. % aqueous solution of oxalic acid in the potentiostatic mode, as described in previous papers [28, 50]. Larger pores or smaller pores can be obtained by anodizing in phosphoric acid or sulfuric acid, respectively [51].

A graphite plate served as the cathode. Anodization of the Al layer proceeded with a nominal current density 4.0 mA/cm². At once after anodizing of aluminium the “thinning” of a barrier layer at the bottom of a pore was carried out at gradual decrease in potential with a constant rate of 0.5 mV/s till 20V. During this processing, the barrier layer local thinning proceeds at the bottom of pore down to the Ti under layer only. The pore diameter (40-50 nm) does not change but barrier layer thinning approximately to 20 nm. The Ti film is not anodized through the porous alumina in these conditions. The remains of a barrier layer deleted just before nickel deposition by cathodic dissolution in electrolyte of Ni deposition at a voltage (-3.0 – 4.0) V (SCE) within (3-5) min as it is described in work [52]. As a result the pores becomes nearly through (barrier layer thinning at the bottom of pore approximately to 7-10 nm). That is, the through pore oxide (with thickness about 1000 nm) disposed on a metal (Ti) film of large thickness (about 500 nm) sufficient to perform the metal electrochemical deposition process. The Ti film with through pores alumina serves as a working electrode under Ni electrochemical deposition at the direct current (*dc*) mode. A similar technique could be incorporated with this structure to electrically address the CNTs.

To deposit Ni into the thin porous Al oxide we used electrolyte of the following composition (in g/l): NiSO₄ · 7H₂O (140); NiCl₂ · 6H₂O (30); H₃BO₃ (25); Na₂SO₄ (60). The electrolyte temperature was 20±2 °C, pH = 5.2. Local deposition was carried out in a three-electrode cell by sweeping the voltage at a constant rate of 20 mV/s from zero to a constant potential in the range -1.6 V (SCE) to -2.0 V (SCE) and then at this potential for (2.0 – 4.0) min (*dc*-electrochemical deposition). The graphite plate as an auxiliary electrode and the silver-chlorine electrode (SCE) as a reference electrode were used. The electrolyte stirring was performed with magnetic stirrer. Anodizing and electrochemical deposition processes control was performed using an Electronic Measurements constant current/constant voltage power supply P-5827 M (potentiostat). Time dependant electrochemical parameters were registered with a digital multimeter linked to PC via a general-purpose interface bus.

CNTs were synthesized using injection CVD method by means of a high-temperature pyrolysis of liquid hydrocarbon xylene [C₈H₁₀] mixed with the volatile catalyst source ferrocene [Fe (C₅H₅)₂]. The process was performed at atmospheric pressure in an Ar/NH₃ flow. Ammonia addition was supposed to facilitate the catalytic activity of Ni clusters at the bottom of a pore at the high temperature synthesis conditions. The ferrocene concentration in xylene was 0.1 wt. %, the injection

rate of the reaction mixture into the reactor zone was 1 ml/min, the temperature was 870 °C, the argon flow rate was 100 cm³/min, and the flow rate of NH₃ was 10 cm³/min. The synthesis duration was 30–60 seconds.

The composite carbon material consisting of the array of the carbon nanotubes which are built in thin porous AAO on Ti contact electrodes was local created. The subsequent thermal annealing in the presence of transitional metal (nickel) at a temperature of 350 °C within 60 min promoted improvement of electric contact between tubes and a metal electrode (Ti).

After CNT synthesis ionic cleaning of a sample surface in the argon atmosphere by bombing with argon ions with energy 3keV was carried out. At ionic etching of sample surface the template material (AAO) is etched quicker, than material of tubes therefore tubes in SEM-photos look over AAO surface. After additional chemical cleaning the samples were washed out in the distilled water up to pH = 6-7.

Surface topography, microstructure and composition of the AAO and carbon nanocomposite have been investigated by scanning electron microscopy (SEM - Philips XL 30 S FEG) and atomic-force microscopy (AFM) using the Nanotop NT-206 ("Mikrotestmashiny", Belarus) installation. The AFM measurements were carried out in a contact mode in atmospheric conditions using the silicon cantilever CSC12/15. Experimental data processing was carried out using the «SurfaceXplorer» software for AFM data processing, visualization and analysis. Given program allows accomplishing of the microstructure research on a series of different-scale images covering all the variation range of structural elements sizes available in the sample. During the analysis, the data on sizes and configuration of structural elements were received, the estimation of their spatial orientation was made, and integrated parameters of the microstructure were calculated. The structural analysis of the Ni nanoparticles (NPs) was obtained from X-ray diffraction (XRD, Rigaku) with Cu K α radiation ($\lambda=0.154056\text{nm}$).

2) Results and Discussion

In Fig. 11 the SEM image (A) and profile of a Ti electrode layer surface (B) with islands of electrochemical deposited nickel after selective etching of AAO are submitted. Various levels of the grey are caused by a different height (uneven) of filling of a pore with nickel: light-grey colour – is closer to an external surface of a sample, darkly grey – is closer to an internal surface of a template. It is connected with non-uniform morphology of a barrier layer surface on the oxide - titan interface as a result of thinning.

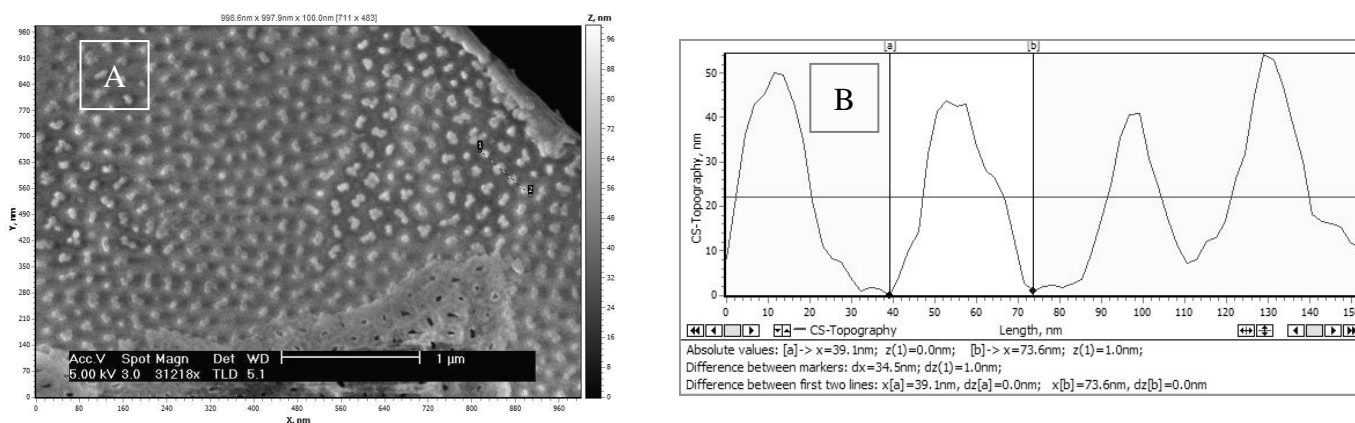


Fig. 11 SEM-photo (A) and profile of a surface of Ti conductor layer (B) with islands of electrochemical deposited nickel after selective etching of AAO

The size of light sites (points) corresponds to the size of catalyst Ni nanoparticles and averages 28 nm. More dark sites round islands of nickel correspond to Ti layer under bottom part of an oxide pore after gradual decrease in anodizing potential till 20V. The size of these areas is close to the size of a pore in the etched oxide. Other dark field is a layer of the titan.

The typical XRD pattern of Ni nanoparticles *dc*-electrodeposited into porous Al₂O₃ is presented in Fig. 12.

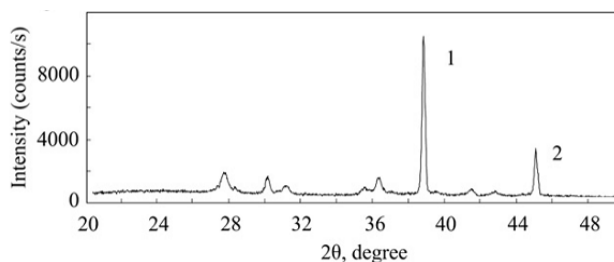


Fig. 12 XRD pattern of Ni NPs *dc*-deposited into porous Al₂O₃; 1- peak corresponding to Ti film; 2- peak of Ni phase

The shape of this XRD data with narrow peaks suggests a crystalline deposit. The nickel phase is crystallized in *fcc*

lattice, as resulted by identification of Ni samples using ASTM reference-calculation tables. Except the main peak (2) of Ni phase ($2\theta = 44.79^\circ$) on XRD patterns there is the peak (1) corresponding to the Ti film ($2\theta = 38.52^\circ$). The template (Al_2O_3) is roentgen-amorphous and does not bring an essential contribution to the diffraction spectrum.

By processing the XRD data, the average size of crystallites was calculated using the Debye–Scherrer equation and the crystallite size ranges from 25.6 nm to 38.8 nm.

In Fig. 13 the top SEM images of the samples after CNT synthesis at 870°C in 0.1% mixtures ferrocene-xylol are shown. Character of a surface topography of these samples is presented in Figs. 14 and 15.

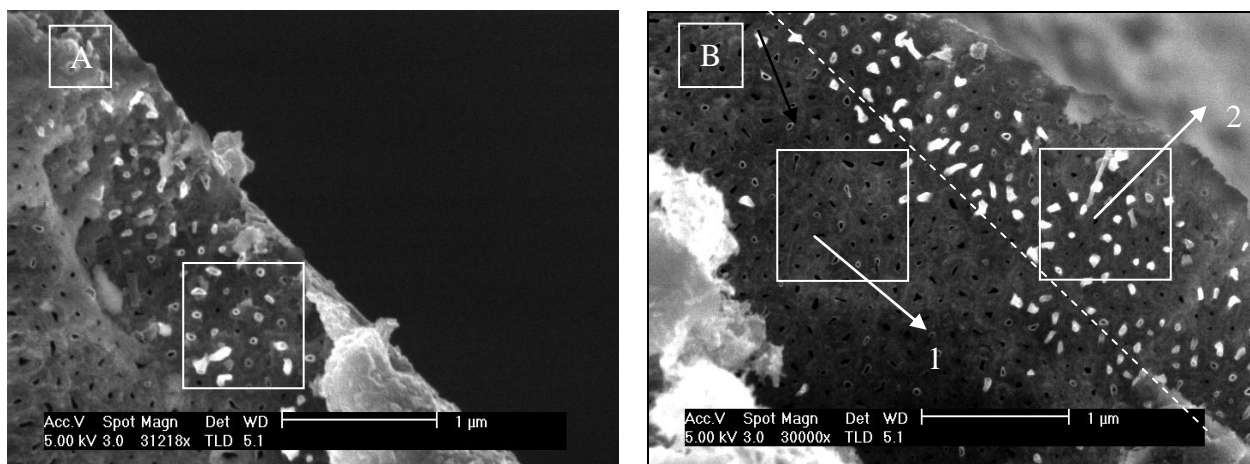


Fig. 13 SEM top view of the surface of two samples received within 40 seconds (A) and 60 seconds (B) of synthesis at 870°C in 0.1% mixture ferrocene-xylol

The conditional boundary (the shaped line) divides two areas of a sample with different degree of AAO filling with carbon tubes. In each area the sites (squares the size $\sim 1 \times 1 \mu\text{m}$) differing in absence (site 1) and existence (site 2) of the stationary catalyst (nickel) are allocated. All other conditions of synthesis of composite material are identical.

Parameters of the CNT array and degree of AAO filling with tubes on different sites of a sample are specified in Table 3.

From Figs. 13-15 and Table 3 it is visible that array of the ordered carbon tubes with high degree of the uniformity of the geometrical sizes which is not exceeding 25% is formed in porous AAO. Key parameter (external diameter of tubes) determined by properties of AAO, but not conditions of synthesis has dispersion about 20%. The nanotubes repeating the pore shape were open-ended, and they did not contain visible structural defects.

Degree of orderliness and uniformity of the geometrical sizes of the CNT array depends on uniformity of the geometrical sizes of the template, i.e. on thickness of AAO and modes of its formation. In that duration of synthesis and thickness of a template ($\sim 1 \mu\text{m}$) a nanotube fill a pore on height completely or slightly come to light out of its limits. The analysis of areas with Ni catalyst and without it shows that presence of Ni increases degree of template filling with carbon tubes.

TABLE 3 PARAMETERS OF THE CARBON NANOTUBES ARRAY IN THIN POROUS AAO

Parameter	Area	
	1 (Fe) [*]	2 (Ni+Fe)
Degree of pore filling, %	10-15	70-85
Outer diameter of CNT d, nm	50 ± 5	50 ± 5
Inner diameter of CNT d ₀ , nm	25 ± 5	20 ± 5
Intertube spacing D, nm	120 ± 10	120 ± 10
Aspect ratio	15	20

^{*}Fe from ferrocene

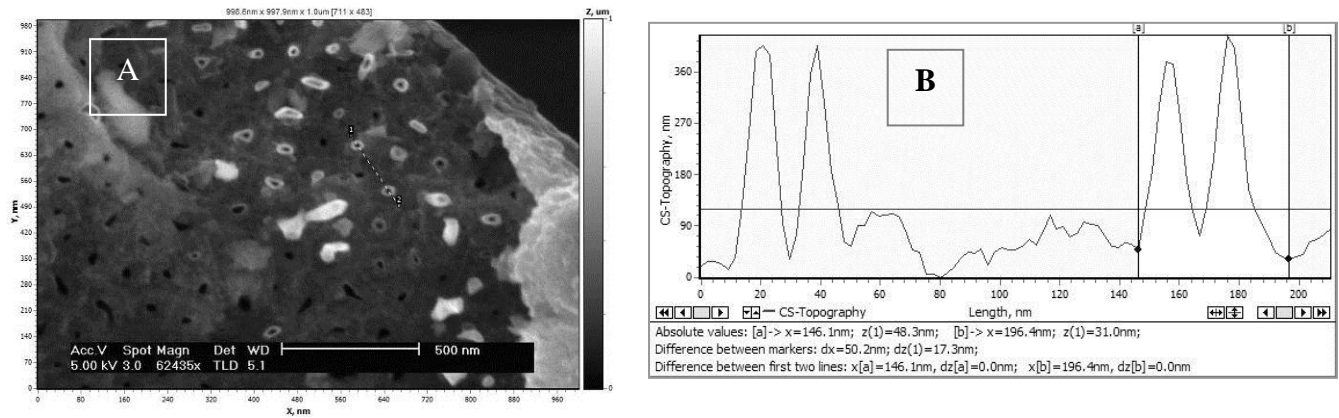


Fig. 14 SEM top view (A) and AFM surface topography (B) of the sample received within 40 seconds of synthesis at 870 °C in 0.1% mixes ferrocene xylol

It is considered that availability of the catalyst is necessary condition for CNT production. The role of the catalyst is reduced to adsorption of initial carbon-bearing composition on a surface of the catalyst NP, dissociation of it, dissolution of carbon in volume of a catalyst NP and the subsequent release of the dissolved carbon with formation of single-wall, multiwall nanotubes or nano fibers [53]. Occurrence of this or that mechanism of CNT growth is defined by many factors among which besides external conditions (temperature, the general and partial pressure, composition of initial compound, etc.) the size and structure of catalyst NPs, character of interaction of the catalyst with the template or a substrate have the predominating role [53].

Different mechanisms of CNT growth, including, in a pore of nanometer size (5-10) nm on catalyst NPs of 1-5 nm size are offered [54] and so far there is no unambiguous opinion concerning the mechanism of CNT growth on the catalyst NPs of the bigger size. It is possible to assume that in this case, (in porous AAO) conditions for synthesis of CNT are similar to synthesis conditions in the one-dimensional nanoreactor (in every pore of AAO) and oxide takes part in this process [37].

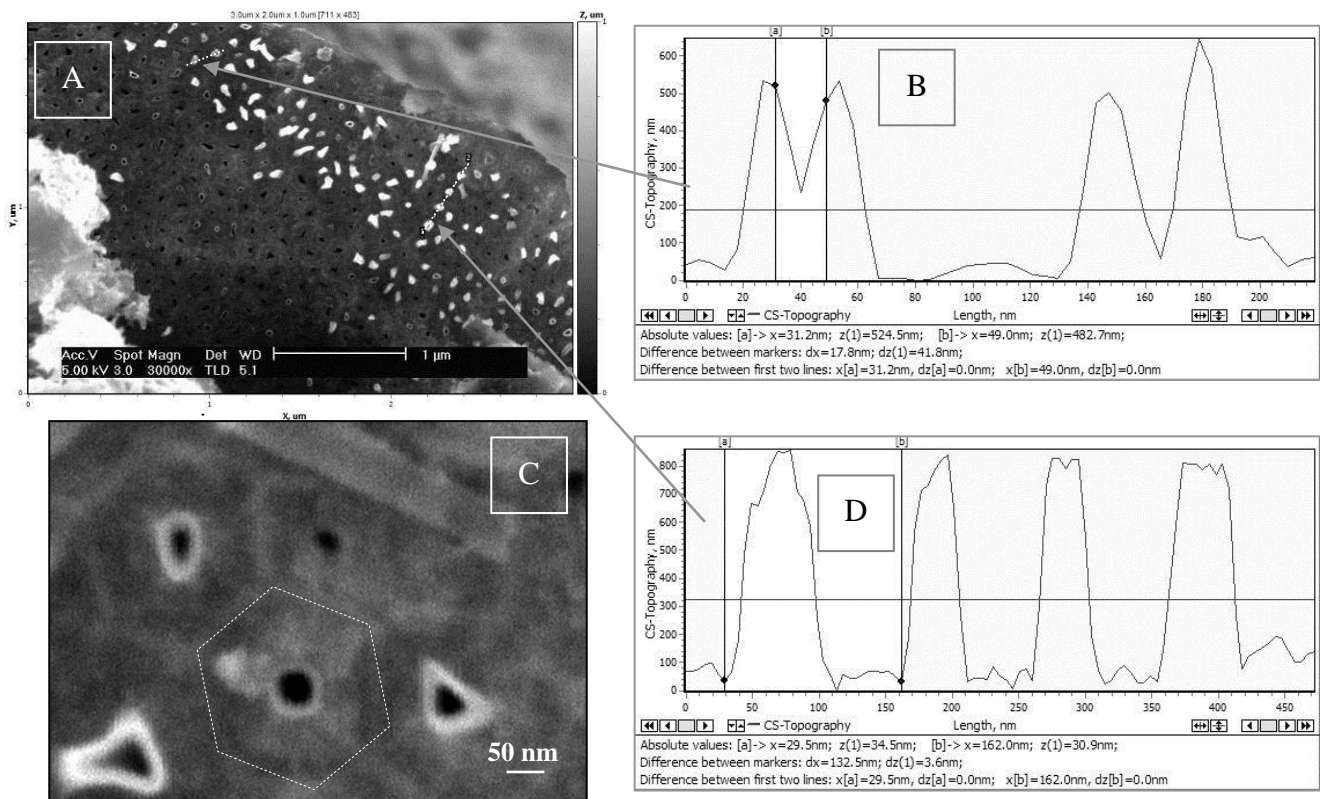


Fig. 15 SEM top view (A), enlarged fragment (C) and AFM surface topography (B, D) of the sample received within 60 seconds of synthesis at 870 °C in 0.1% mixes ferrocene xylol

In the received samples the size of carbon tubes is close to the size of a pore of AAO. In the absence of the stationary catalyst, site 1 on Fig. 13(B), carbon tube can grow on the flying catalyst (iron) NPs. At pyrolysis of ferrocene fine particles of iron (NP) are formed. Having the insignificant sizes, particles are in a suspension and penetrate into the some of AAO pore therefore degree of filling of a pore on this site is very small. But the probability of penetration of randomly moving

particles inwards a narrow pore of oxide is very small.

On sites with nickel clusters at the bottom of a pore (site 2, Fig. 13) MWCNT are formed at thermal decomposition of molecules of xylol, $C_6H_4(CH_3)_2$, and ferrocene, $(C_5H_5)_2Fe$, at temperature of 870 °C. As a result of heating the hydrocarbon molecules are split on reactionary-active radicals. The received carbon-bearing radicals migrate along a pore surface and enter in chemical reaction to internal surface of a pore therefore occurs formation of a carbon film. As the lattices of γ - Al_2O_3 and graphite significantly differ in size of constant lattices (0.79 and 0.25 respectively), it is difficult to assume that crystal structure features of this graphite material is define by atomic structure of an oxide surface on walls of a pore. Most likely, origin of graphite crystallite happens on an annealed surface of a pore which promotes effective fixing of carbon atoms. Tubes in which walls consist of layered crystal grain of graphite are formed. In literature such tubes designate multilayered carbon nanotubes (MWCNTs) with structure like such as “papier-mache” [55-57].

Unfortunately, results of TEM investigation of side sections of the allocated tubes did not allow interpreting unambiguously structure of walls of the received carbon tubes. It is connected with that rather difficult to receive SEM images of face cuts of multilayered nanotubes, and images of lateral sections allow various interpretation.

Investigation by means of KR-spectroscopy, Fig. 16, showed that at typical Raman spectrum there is a band at 1595 cm^{-1} corresponding to twice degenerate deformation fluctuations of an element of graphene structure and the band at 1360 cm^{-1} corresponding to vibration conditions of the destroyed hexagonal lattice near borders of carbon crystallites. Existence of two peaks at these frequencies with comparable intensity is characteristic for the graphitized materials consisting from the disordered carbon nanocrystallites [58], carbon nanofibres [59] or carbon nanotubes with high degree of deficiency of graphene walls.

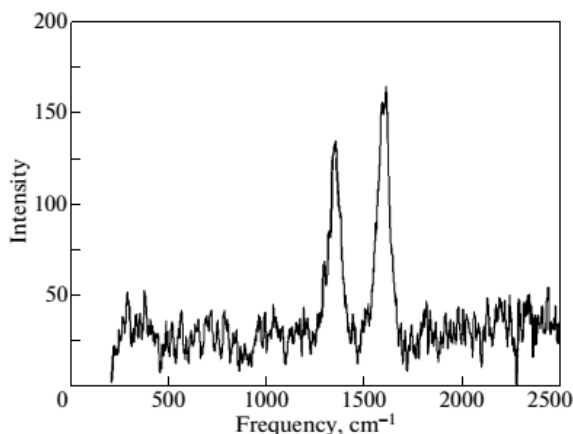


Fig. 16 Raman spectrum ($\lambda=532\text{ nm}$) of the received MWCNT after the surface cleaning

3) Conclusion

Process of formation of vertically aligned carbon nanotubes localized on metal electrodes with use of thin porous AAO on various functional substrates is presented.

Advantages of the developed process are technological effectiveness; wide range of varying of syntheses structure parameters. Besides, this process can be carried out with use of equipment, traditional for semiconductor technology.

The received composite material representing the array of vertically aligned carbon nanotubes localized on metal electrodes which are built in porous oxide of aluminum possesses high sorption ability, chemical and mechanical firmness. It will allow creating the microchips, for example, electrode biosensors providing direct electric measurements with use of nanodimensional sensitive elements (electrodes) of Faradaic and non-Faradaic impedance biosensors for bacterial detection without redox probes [60-62]. Such measuring modules are already manufactured on the basis of nanoporous oxide of aluminum. However their use is interfaced to a number of difficulties, in particular to providing conditions of a laminar current of an inoculated nutrient medium along measuring electrodes of capacitor sensors, and also their sterilization [63]. It is supposed that the carbon nanotubes filling channels in AAO will provide not only protection of an internal surface of electrodes at repeated use, but also will allow to maximize information signal, to increase sensitivity and to reduce the volume of the tested sample [15, 64-67].

The carbon cover in every pore protects oxide from dissolution and interaction with chemical reactants, keeping its specific properties. It also provides biocompatibility and stability in many organic and inorganic environments and, besides, interferes with absorption of moisture from the atmosphere that is characteristic for usual porous aluminum oxide. Such carbon composites possessing considerable resistance to electrochemical corrosion are steady also against radiation in hostile environment.

Supposedly the mechanism of CNT formation in AAO is based on interaction of carbon dimers with a surface of walls of crystal AAO at high temperature both in areas with the catalyst and in areas without it. But unlike growth mechanism in a free membrane with a through pore, the catalyst (nickel) also plays a certain part. Therefore at the following stage of investigation the task to reduce the sizes of the catalyst particles was set. Results are presented in the following paragraph.

B. CNT with Small Diameter (10 – 25 nm) Synthesized by CVD within the Etch Pore of Thin AAO Template

1) Introduction

Vertical aligned carbon nanotubes have been grown using two type of a thin porous AAO template. In the one type of AAO-1 there is no catalyst in the pore and in the two type of AAO-2 there are catalyst nanoparticles (NP). The initial film structure consisted of an electrode Ti layer and a basic Al layer, deposited on a Si, Si/SiO₂ or ceramic substrate. The Al layer was anodized to create a self-ordered pore structure. CNTs were synthesized by high-temperature chemical vapor deposition. The catalyst NPs of Ni with dimensions 15 ± 5 nm was formed using electrochemical deposition on an alternating current (*ac*-mode).

Depend of the surface properties of pore walls different type of CNT arrays growth within the pores of thin AAO. In AAO-1 generated multiwall CNT (MWCNT) that take the diameter of the AAO pore from which they originate (typically 50–100 nm). And MWCNT with small-diameter (10 – 25 nm) was observed within the etch pore of AAO-2.

AAO template have been used in the synthesis of vertically oriented multi-walled CNTs (MWCNT) [68-70] and MWCNT devices [71] that take the diameter of the AAO pore from which they originate typically 50–100 nm [70, 71]. These synthesis methods proceed using a catalyst metal electrodeposited into the bottom of pores [67-70, 72] or by direct carbon deposition on the template wall, using no metal catalyst [72, 73, 74, and 75]. In this case an inner surface of the AAO pores played the forming and catalytic role. Reported MWCNT synthesis methods utilizing a catalyst include the use of Co [76] or Ni [77] deposited within the pores followed by MWCNT synthesis. These processes yield MWCNTs that take on the diameter of the pores and typically have a high concentration of disordered carbon, but they provide excellent control of the length and diameter of the MWCNTs by varying the dimensions of the AAO [37, 78].

However, single-walled carbon nanotubes (SWCNT) and small-diameter MWCNTs synthesis from customized templates or catalysts is more difficult because of their relatively high activation energy in comparison to typical MWCNTs [79]. Nucleation of such CNTs requires catalyst particles of smaller diameters (about a few nanometers). This size is not easily achieved when incorporation a catalyst within an every pore of a template.

Other approach of creation of vertical CNTs is discussed in works [79, 80]. The template is similar to that of AAO, with the addition of a CNT catalyst metal film (Al/Fe (10 nm thickness)/Al) embedded directly into the AAO film structure, Fig. 17(A-C). CNT synthesis occurs in a microwave plasma enhanced chemical vapor deposition (PECVD) system. Only one CNT is observed emerging for each catalytically active pore, but less than 10% of pores generate CNTs for the film configurations producing the highest density. In addition elimination of the film at the Al/Fe/Al interface often occurred when anodizing films with Fe layers greater than 10 nm. The reproducible production of such thin layer is also ambiguously.

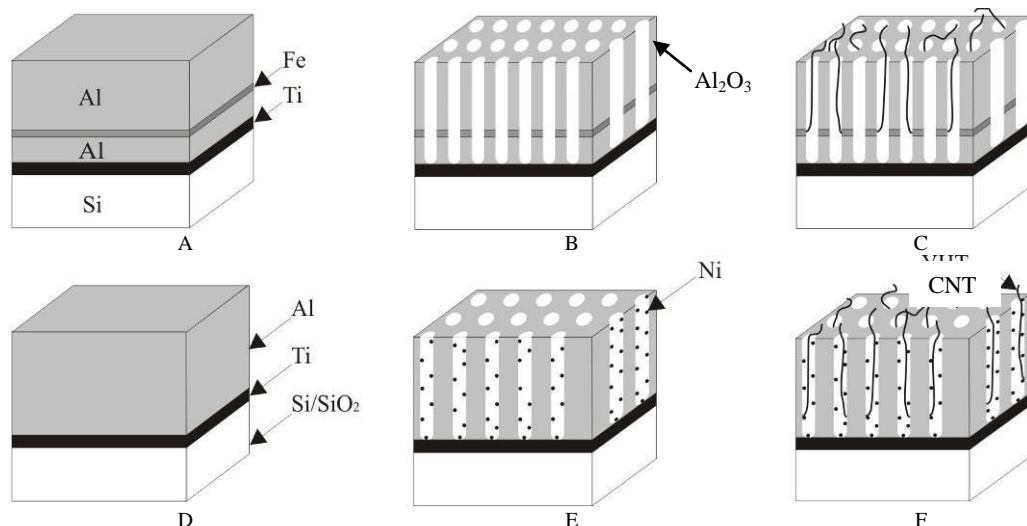


Fig. 17 Schematic diagram of catalyst preparation and CNT synthesis procedure: (A – C) - from [78], (D – F) - authoring; A, D – initial deposited film structure; B, E – anodized film structure; C, F – CNTs synthesized from pore channels

We present a process for obtaining well-ordered individual vertical CNT using a catalyst NPs embedded within the pores of AAO template, Fig. 17 (D-F), and compare it with synthesis of MWCNT in AAO without catalyst. The initial film structure consisted of an electrode Ti layer, and a basic Al layer, deposited on a Si, Si/SiO₂ or ceramic wafer (D). The Al

layer was anodized to create a vertically oriented pore structure (E). The catalyst NPs of Ni with dimensions 15 ± 5 nm were formed using electrochemical deposition on an alternating current (E – *ac* electrochemical deposition). CNTs were synthesized from the catalyst NPs by high-temperature chemical vapor deposition (F).

These self-aligned CNTs differ from previously reported CNTs in thin AAO [79-81] as they have a potential density of 128 CNTs/ μm^2 with a CNT–CNT spacing of 110 ± 5 nm. Dawn and top contacts can be produced using electrochemical and physical vapor deposition, respectively. The length of the CNTs is controlled using different height AAO with a variability of ± 10 nm. The resulting nanostructure is expected to form the basis for development of vertically oriented CNT-based electronics and sensors.

2) Experiment

The initial experimental samples represented two-layer Ti and Al thin film compositions on 6.0×4.8 cm² ceramic or 76 mm diameter Si and Si/SiO₂ substrates, that are same as was already presented in the previous paragraph.

The top layer of Al was anodized to the Ti layer by two-step anodizing process in 4.0 wt. % aqueous solution of oxalic acid in the potentiostatic mode. As larger diameter pores were desired after anodization, it was carried out chemical etching of a barrier layer and widening of a pore as it is described in work [52]. As a result of isotropic chemical etching, increase in pores diameter happens - almost twice from 45 ± 5 nm to 75 ± 5 nm, and barrier layer thinning at the bottom of pore approximately to 7-10 nm.

That is, the through pore oxide disposed on a metal (Ti) film of large thickness (in our case 456 nm) sufficient to perform the metal electrochemical deposition process. The Ti film with through pores alumina serves as a work electrode under Ni electrochemical deposition in the *ac* mode.

The catalyst NPs of Ni with dimensions 15 ± 5 nm was formed using *ac*-electrochemical deposition. For this purpose was used the following electrolyte (in g/l): NiSO₄ × 7H₂O (140) + NiCl₂ × 6H₂O (30) + H₃BO₃ (25) + Na₂SO₄ (60).

The electrolyte temperature was 293 K, pH = 5.2. Deposition was carried out in a two-electrode cell. The graphite plate was used as an auxiliary electrode. Various deposition modes have been investigated to determine optimum parameters of *ac*-deposition: frequency – 180 Hz, voltage – 3 V, current density – 10 mA/cm², deposition duration – 2 min.

Anodizing and electrochemical deposition processes were controlled with the Electronic Measurements galvanostatic/potentiostatic power supply P-5827M (potentiostat) and the special set of low-frequency signal generator GZ-123, correspondingly. Time dependent electrochemical parameters were registered with a PC-connected digital multimeter.

CNTs were synthesized using CVD method by means of a high-temperature pyrolysis of liquid hydrocarbon Decane [C₁₀H₂₂]. This process was performed at atmospheric pressure in an Ar/NH₃ flow. Ammonia addition was supposed to facilitate the catalytic activity of Ni particles at the high temperature synthesis conditions. The temperature in the reaction zone was fixed to 1170 K and the growth duration was in the 1–10 min range. More details about the sample preparation could be found elsewhere [37, 82].

The crystal structure of Ni NPs was studied by X-ray diffraction using a modified DRON-3M diffractometer with CuK α radiation ($\lambda = 0.154242$ nm) as described in [83]. Measurements were performed at room temperature with the step in angle $\Delta 2\theta = 0.03^\circ$.

3) The Features of *ac* Deposition of Ni NPs into the Thin AAO

The catalyst Ni NPs were locally embedded into the AAO, allowing for exposure to reactive gases during CNT synthesis. It is believed that alumina surrounds the catalyst particles, impeding aggregation of the catalyst and enabling retention of catalytic activity for CNT synthesis [78, 82].

Results of Ni *ac*-deposition into the AAO are given in the SEM images of Fig. 18.

It is evident from the photos (Fig. 18(A)-(B)) that Ni is deposited discretely along the pore in the form of spherical-like NPs (light spots in Fig. 18(B)). That is deposition begins not with a bottom of a pore, as at deposition on a direct current (*dc* mode), but along walls of a pore from a bottom to a surface. Perhaps, it is connected with processing of an internal surface of a pore in 4% H₃PO₄ water solution (procedure of widening of pores) and/or endurance of a sample before deposition in nickel plating solution (2-3 min). Expansion of pore diameter is necessary for improvement of conditions of hydrocarbon polyatomic molecules transport during CNT synthesis.

While increasing the deposition time the conglomerates of Ni NPs start to be growth and gain a form of rods, gradually filling a pore. Thus SEM analysis has revealed formation of porous alumina/nickel nanocomposite with characteristic sizes of Ni NPs in the 15–25 nm range at initial stages of Ni *ac*-deposition.

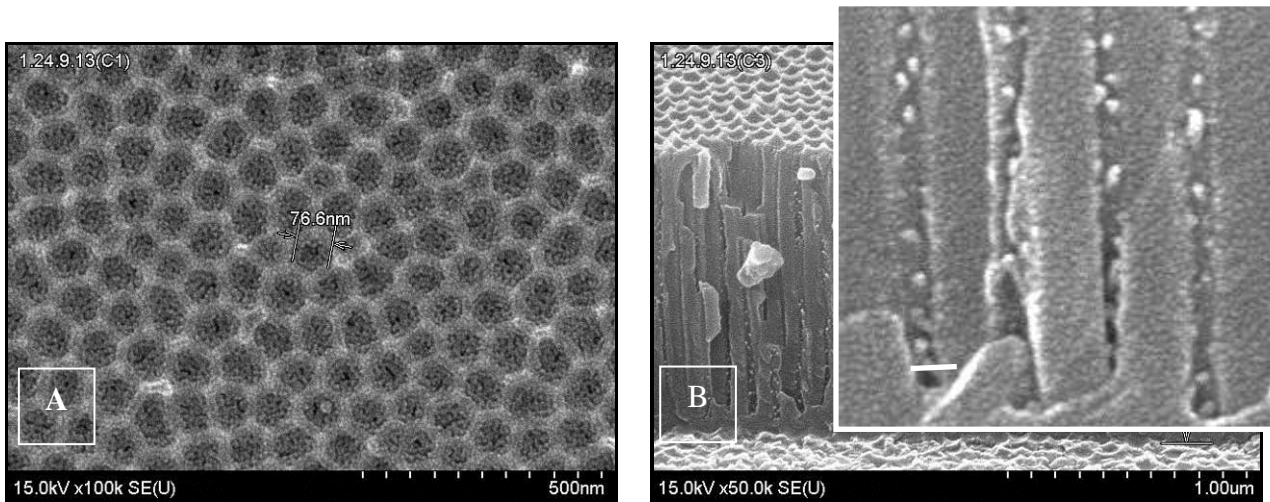


Fig. 18 SEM normal top view (A) and cross-section view (B) of experimental sample after Ni *ac*-deposition and the enlarged image (insert in figure, (scale bar 40 nm)): the deposition was carried out at optimum mode - 180 Hz, 3 V, 10 mA/cm², and deposition duration - 2 min

The crystal structure of Ni NPs in Al₂O₃ was studied by X-ray diffraction. The typical XRD pattern of Ni NPs *ac*-electrodeposited into the AAO on Ti layer is presented in Fig. 19.

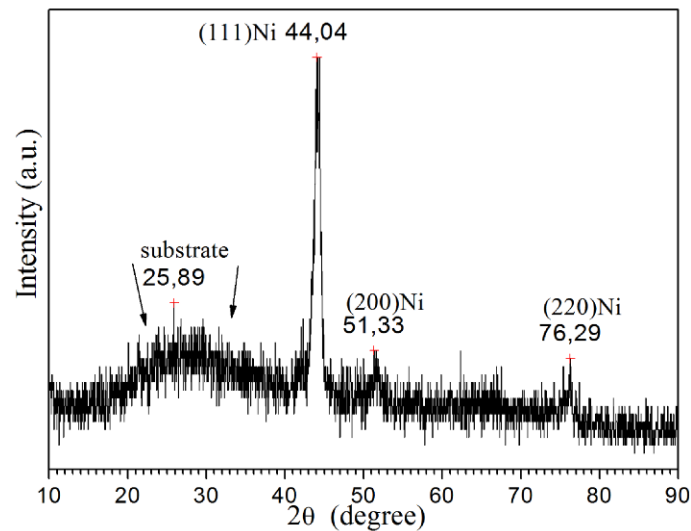


Fig. 19 XRD pattern of Ni NPs *ac*-electrodeposited into the AAO

The shape of this XRD data with narrow peaks suggests a crystalline deposit. The nickel phase is crystallized in *fcc* (*face-centered cubic*) lattice with the orientations (111), (200) and (220), but Ni (111) phase is dominant. These orientations are typical for electrodeposited Ni nanowires [84]. The template is roentgen-amorphous (wide peak at $2\theta = 25.89^\circ$) and does not possibility to see the peak corresponding to the reflection (002) of the titanium ($2\theta = 38.52^\circ$).

By processing the XRD data, the average size of Ni (111) crystallites was calculated using the Debye–Scherer equation. The crystallite size of Ni NP ranges from 15.6 nm.

4) Results of CVD Synthesis Individual CNT from within a Thin AAO Template

Results of CVD synthesis individual CNT from within a thin AAO template are given in the SEM images of Figs. 20 and 21.

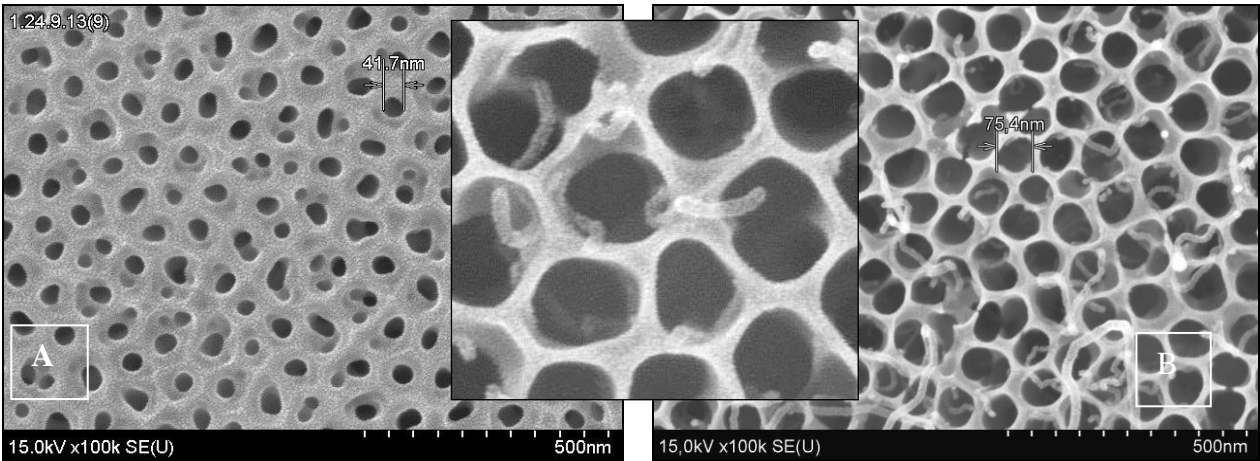


Fig. 20 SEM top images of the experimental sample after through anodization (A), after CNT growing from AAO pores (B) and enlarged fragment of this photo (insert)

Small-diameter CNTs (10 – 25 nm) can be observed within the pore structure after CVD synthesis. Lengths of these CNTs exceed one micron¹. In spite of obtaining length exceeding one micron (aspect ratio more than 50), CNTs and small CNT bundles maintain a vertical orientation or have the appearance of vertically oriented loops. Some horizontally oriented CNTs are observed on the top AAO surface (Fig. 21(A)).

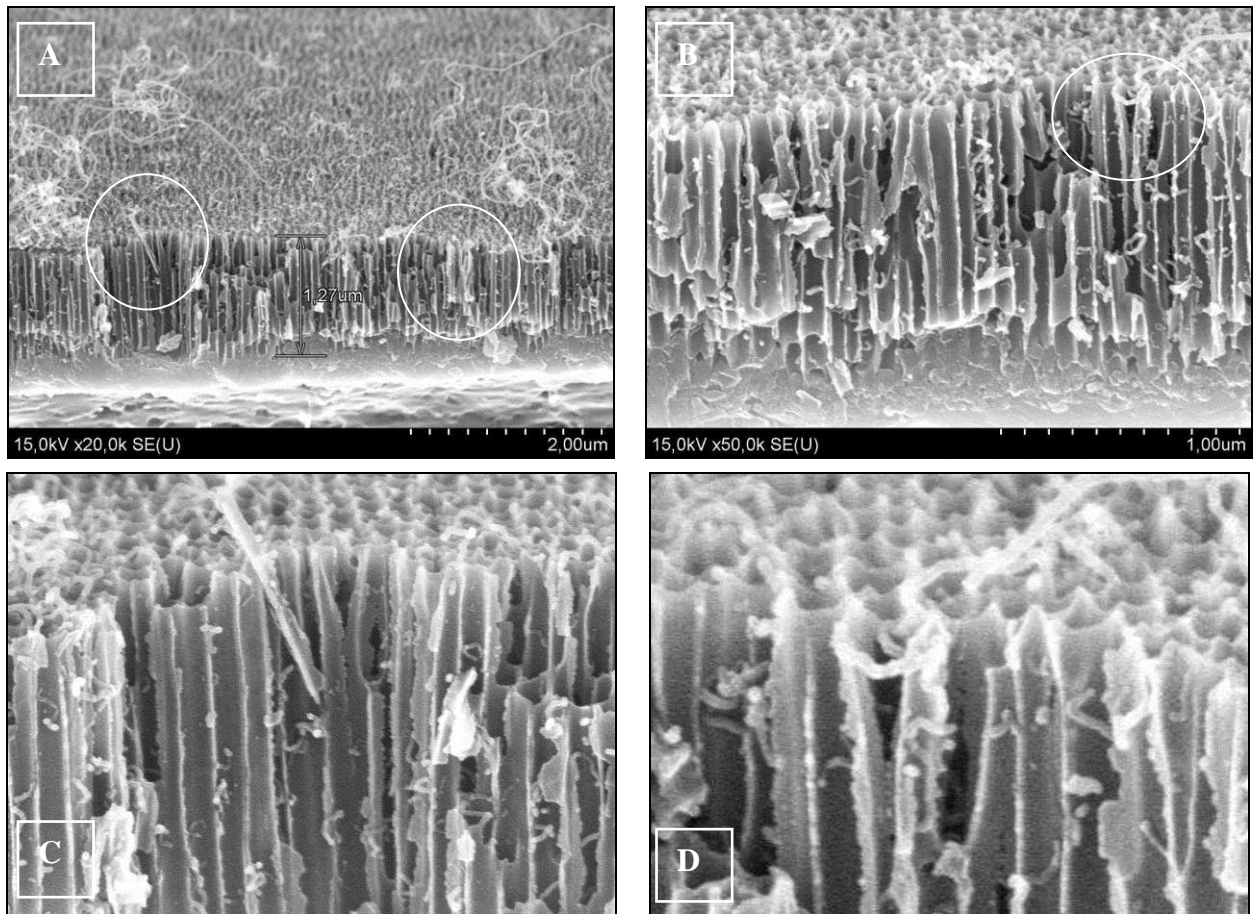


Fig. 21 Cross-sectional SEM views of CNT growing vertically from PAA pores in different magnification (A, B) and enlarged fragments of these photos (C, D)

It should be noted that the cross-sectional SEM images were obtained by cleaving the AAO, thereby occur detachment of the CNTs from their pores of origin. As a result, identifying the origin of CNTs within the pores using cross-sectional

¹ The oxide height in this sample is equal to 1.27 microns

views is difficult, although several such images are shown in Fig. 21(A, C) – they are outlined by circles. Numerous CNTs may be observed emerging from their pores of origin, however, by scanning the top AAO surface, as can be seen from Fig. 20.

According to observations only one CNT nucleates in any given pore, despite that in every pore there is a set of Ni particles. We assume that it is caused by limited gaseous-carbon supply and the relatively high activation energy required for nucleation [80]. It is significant that a nanotube arises on Ni (111) NPs which are in the interior of pores (on one of particles located close with a pore wall) and do not arise on nickel NPs which are on a relief surface of oxide. Apparently the conditions, necessary for a nanotube nucleation, exactly here are created. In some works [85, 86], it is noted that under such conditions, each pore may be considered as a sub miniaturized chemical reactor wherein polyatomic molecules move. Such an approach offers the advantage of concentrating the reagents and catalysts in a limited volume with the isolation of the reagents from the outside ambient.

CNT proceeds to grow vertically to the surface of the AAO toward the carbon supply after nucleating. Supporting evidence of this vertical growth is evident in top and cross-sectional SEM images showing freestanding, vertical CNTs.

The generation of CNT-bundles further complicates locating the pore of origin of individual CNTs. Therefore quantification of CNT population density from AAO pores using SEM imaging was produced with respect to the normal top view (focal plane) (Fig. 20). We estimate that approximately 70%² of pores generate CNTs for the film configurations producing the highest density, and only one CNT is observed emerging for each catalytically active pore. According to preliminary data number density and length of CNT depends on a regularity of AAO, the mode of Ni NPs *ac*-deposition and the duration of CNT synthesis under other conditions being equal. More detailed investigations regarding the correlation between of CNT number density and conditions of nanocomposite synthesizes with different metal NPs in progress now.

TEM images of individual MWCNT for two different samples, such as those shown in Fig. 22, reveal a mixture of MWCNTs with small diameter from 10 to 25 nm. Samples for TEM analysis were prepared by CNTs dispersion from the template using a sonication in isopropyl alcohol for 20 min followed by centrifugation for 10 min.

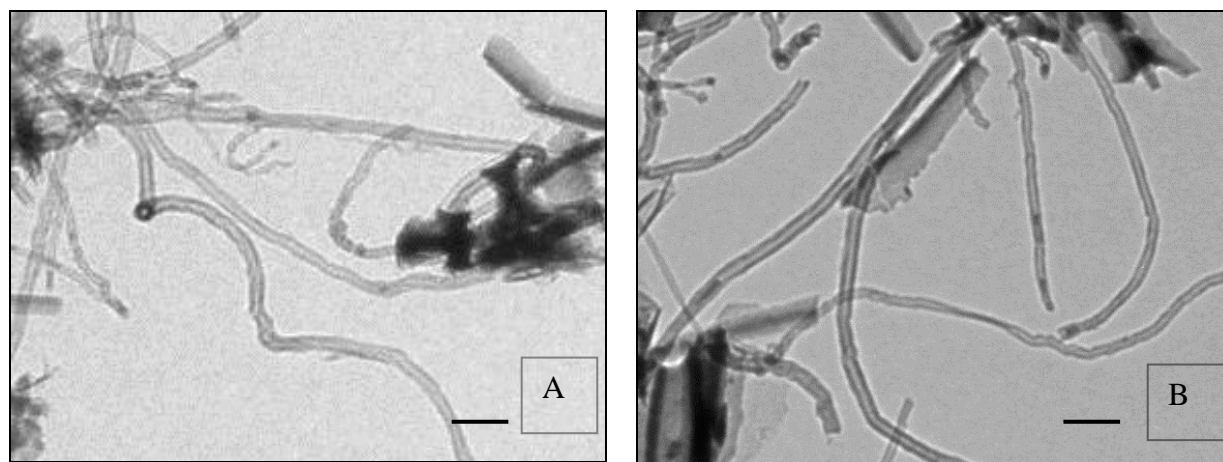


Fig. 22 TEM images of MWCNT. Scale bar = 40 nm

Further optimization of Al film anodization (regularity), Ni NPs *ac*-electrodeposition (size of NPs reduction) and CNTs synthesis conditions are expected to increase CNT number density and to improve their quality. Majority of the CNTs emerging from the top AAO surface are vertically oriented, but alignment uniformity would likely benefit from application of a negative substrate bias using PECVD synthesis [87].

For the investigation of the nanotube structure, the samples were studied by Raman spectroscopy. Fig. 23 shows the typical Raman spectrum of MWCNT locally growing in AAO on ceramic substrate.

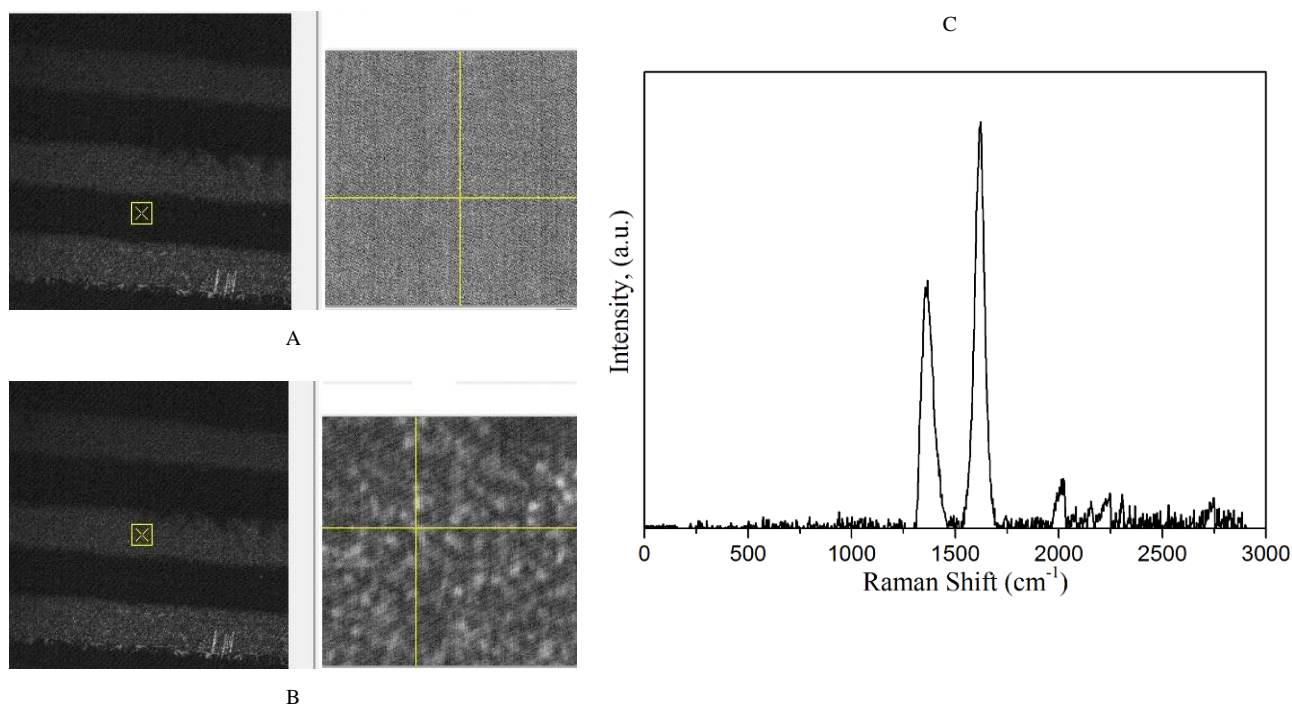


Fig. 23 Top SEM images of the experimental sample (A, B) and Raman spectrum ($\lambda = 473$ nm) of the received MWCNT (C) in place indicated on photo (B)

Raman spectrum exhibited two distinct peaks at 1361 and 1618 cm^{-1} which are the feature of disordered and graphitic carbon (D and G bands), respectively. The band at 1550 - 1620 cm^{-1} (G band) is attributed to E_{2g} symmetry in-plane optical mode associated with the stretching of all C=C pairs. While the band near 1361 cm^{-1} (D band) physically related to the in-plane A_{1g} symmetry breathing mode of the C hexagon which intensifies and broadens when increases amount of structural defects. The intensity ratio IG/ID, as a first metric for CNT quality, is approximately 2, indicating relatively high-quality CNTs. It is noted that the increased intensity of a D band can be caused by a large number of short tubes in which edge effects exhibit most significantly.

For comparison the SEM images of the top-view of the MWCNT synthesized without floating catalyst (A) and by floating catalyst CVD method (B) in the thin AAO on a Si/SiO₂ substrate are shown in Fig. 24.

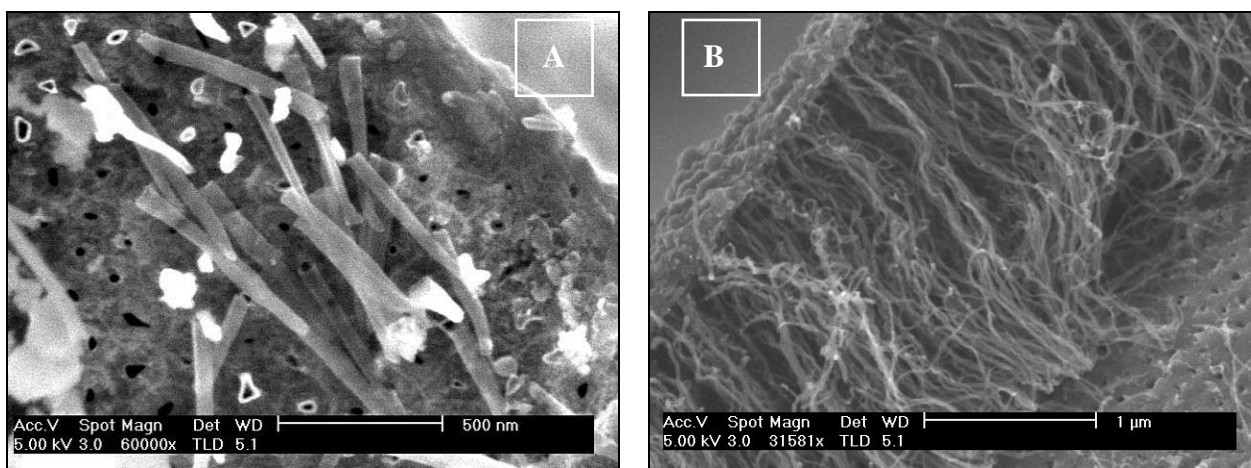


Fig. 24 SEM images of the top view of the MWCNT synthesized without floating catalyst in xylol³ (A) and by floating catalyst CVD method in 0.1% mixed ferrocene-xylol (B) at 1123K

In the first case MWCNTs take on the diameter of the pores (55-65 nm) and provide control of the length and diameter of the MWCNTs by varying the dimensions of the AAO. Nanotubes keep a form and the sizes after selective etching in an aggressive solution on the basis of hydrofluoric acid and possess high chemical and mechanical resistance. In the second case MWCNTs array was formed on the surface of AAO. Each CNT has the diameter about 20 nm and the same distance

³ After chemical etching of AAO

between them.

The received nanotubes (Figs. 20-22) differ from presented in Fig. 24(B) that have small diameter but large distance between tubes (as in the case in Fig. 24(A)). Arrays from MWCNTs with such advantages are of essential interest as active elements in field-emission cathodes and chemical and biological sensor.

5) Conclusion

A thin AAO template with a localized catalyst Ni (111) NPs embedded into the pores by means of *ac*-electrodeposition has been used for the first time to synthesize individual vertical aligned CNTs. TEM and Raman spectroscopy reveal that relatively high-quality MWCNTs with small diameter (10-25 nm) are synthesized. SEM analysis reveals CNTs initiating from the catalyst Ni NPs and emerging from their pores of origin. The structure contains a conductive Ti layer underneath the AAO template to serve as the contact electrode for future electrodeposition of metal nanopillars to electrically address the bottom surface of the CNTs.

CNT number density is equal to 90 CNTs/ μm^2 and depends of the thickness and uniformity of AAO. Influence of a matrix on the mechanism of growth of CNT in porous oxide is studied.

We have developed a simple and highly flexible reproducible method to locally fabricate ordered CNT arrays in thin porous alumina template on various substrates. Further processing and optimization of the structure are expected to enable densely packed CNT-based electronic and sensing devices by functionalization of the CNTs within the vertical self-ordered pore templates.

ACKNOWLEDGMENTS

The authors thank Prof. L.J. Balk and Dr. R. Heiderhoff (Bergische Universität Wuppertal) for the admission to the scanning electron microscope and Dr. K.I. Yanushkevich (Institute of Semiconductor and Solid State Physics, National Academy of Sciences, Belarus) on assistance of X-ray diffraction investigations.

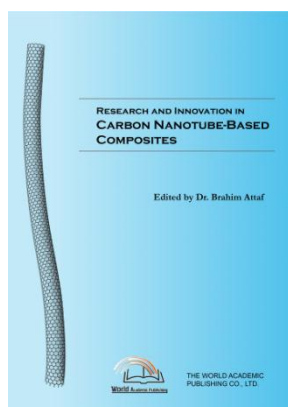
REFERENCES

- [1] Wenchong Hu, Dawei Gong, and Zhi Chen, "Growth of well-aligned carbon nanotube arrays on silicon substrates using porous alumina film as a nanotemplate," *Appl. Phys. Lett.*, vol. 79(19), pp. 3083-3085, 2001.
- [2] A.I. Vorobyova and E.A. Outkina, "Study of pillar microstructure formation with anodic oxides," *Thin Solid Films*, vol. 324(1-2), pp. 1-10, 1998.
- [3] S. Shingubara, "Fabrication of nanomaterials using porous alumina templates," *Journal of Nanoparticle Research*, vol. 5, pp. 17-30, 2003.
- [4] M. Cheng and H. Junhui, "Confined conversion of CuS nanowires to CuO nanotubes by annealing-induced diffusion in nanochannels," *Nanoscale Res. Lett.*, vol. 6, pp. 150-156, 2011.
- [5] Poinern Gerrard Eddy Jai, Ali Nurshahidah, and Fawcett Derek, "Progress in nano-engineered anodic aluminum oxide membrane development," *Materials*, vol. 4(3), pp. 487-526, 2011.
- [6] A.I. Vorobjova, "Electronics elements on carbon nanomaterials," *Uspekhi Sovremennoy radioelektroniki (Advances in present radio electronics)*, vol. 7, pp. 41-67, 2013.
- [7] A.I. Vorob'eva, "Fabrication techniques of electrode arrays for carbon nanotubes," *Uspekhi Fizicheskikh Nauk (Advances in Physical Sciences)*, vol. 179(3), pp. 243-253, 2009.
- [8] Tatsuya Iwasaki, Taiko Motoi, and Tohru Den, "Multiwalled carbon nanotubes growth in anodic alumina nanoholes," *Appl. Phys. Lett.*, vol. 75(14), pp. 2044-2047, Oct. 1999.
- [9] R. Angelucci, I. Boscolo, A. Ciorba, M. Cuffiani, et al., "Honeycomb arrays of carbon nanotubes in alumina templates for field emission based devices and electron sources," *Physica E*, vol. 42, pp. 1469-1476, 2010.
- [10] A. Angelucci, A. Ciorba, L. Malferrari, F. Odorici, R. Rizzoli, M. Rossi, V. Sessa, M. Terranova, and G. Veronese, "Field emission properties of carbon nanotube arrays grown in porous anodic alumina," *Phys. Status Solidi (c)*, vol. 6(10), pp. 2164-2169, 2009.
- [11] D. Li, Y. Cheng, M. Cai, J. Yao, and P. Chang, "Uniform arrays of carbon nanotubes applied in the field emission devices," *Science China Physics, Mechanics and Astronomy*, vol. 56, pp. 2081-2088, 2013.
- [12] R.J. Chen, S. Bangsaruntip, K.A. Drouvalakis, et al., "Noncovalent functionalization of carbon nanotubes for highly specific electronic biosensors," *Proc. Nat. Acad. Sci. USA*, vol. 100, pp. 4984-4989, 2003.
- [13] R. Mangu, S. Rajaputra, P. Clore, D. Qian, R. Andrews, and V.P. Singh, "Ammonia sensing properties of multiwalled carbon nanotubes embedded in porous alumina templates," *Materials Science and Engineering: B*, vol. 174, pp. 2-8, 2010.
- [14] Z. Jin, F. Meng, J. Liu, M. Li, L. Kong, and J. Liu, "A novel porous anodic alumina based capacitive sensor towards trace detection of PCBs," *Sensors and Actuators B: Chemical*, vol. 157, pp. 641-645, 2011.
- [15] H. Orikasa, N. Inokuma, S. Itisanronnachai, X.H. Wang, O. Kitakami, and T. Kyotani, "Template synthesis of water-dispersible and magnetically responsive carbon nano test tubes," *Chem. Commun. (Cambridge)*, vol. 19, pp. 2215-2219, 2008.
- [16] H. Gao, X. B. Wu, J. T. Li, G. T. Wu, J. Y. Lin, K. Wu, and D. S. Xu, "Hydrogen adsorption of open-tipped insufficiently graphitized multiwalled carbon nanotubes," *Appl. Phys. Lett.*, vol. 83, pp. 3389-3394, 2003.

- [17] X.Y. Zhang, L.D. Zhang, G.H. Zheng, and L.X. Zhao, "Template synthesis of high-density carbon nanotube arrays," *J. of Crystal Growth*, vol. 223, pp. 306-310, 2001.
- [18] J.Y. Miao, Y. Cai, Y.F. Chan, P. Sheng, and N.A. Wang, "A novel carbon nanotube structure formed in ultra-long nanochannels of anodic aluminum oxide templates," *J. Phys. Chem.*, vol. 110(5), pp. 2080-2083, 2006.
- [19] K. Yu, G. Ruan, J. Ben, and J. Zou, "Synthesis of carbon nanotubes within Pt nanoparticles-decorated AAO template," *Mater. Lett.*, vol. 61, pp. 97-100, 2007.
- [20] S. H. Jeong and K. H. Lee, "Fabrication of the aligned and patterned carbon nanotube field emitters using the anodic aluminum oxide nano-template on a Si wafer," *Synth. Met.*, vol. 139, pp. 385-390, 2003.
- [21] W. C. Hu, L. M. Yuan, Z. Chen, D. W. Gong, and K. Saito, "Fabrication and characterization of vertically aligned carbon nanotubes on silicon substrates using porous alumina nanotemplates," *Nanosci. Nanotechnol.*, vol. 2, pp. 203-207, 2002.
- [22] H. Gao, C. Mu, F. Wang, D. Xu, K. Wu, Y. Xie, S. Liu, E. Wang, J. Xu, and D. Yu, "Field emission of large-area and graphitized carbon nanotube array on anodic aluminum oxide template," *J. Appl. Phys.*, vol. 93, pp. 5602-5607, 2003.
- [23] W. J. Yu, Y. S. Cho, G. S. Choi, and D. Kim, "Patterned carbon nanotube field emitter using the regular array of an anodic aluminium oxide template," *Nanotechnology*, vol. 16, pp. 291-295, 2005.
- [24] S. Hofmann, G. Csanyi, A.C. Ferrari, M.C. Payne, and J. Robertson, "Surface diffusion: The low activation energy path for nanotube growth," *Phys. Rev. Lett.*, vol. 95(036101), pp. 1-4, 2005.
- [25] M.R. Maschmann, A.D. Franklin, T.D. Sands, and T.S. Fisher, "Optimization of carbon nanotube synthesis from porous anodic Al-Fe-Al templates," *Carbon*, vol. 45(11), pp. 2290-2296, 2007.
- [26] J. Zuidema, X. Ruan, and T.S. Fisher, "Optical properties of ordered carbon nanotube arrays grown in porous anodic alumina templates," *Optics Express*, vol. 21(19), pp. 22053-22062, 2013.
- [27] H. Masuda and K. Fukuda, "Ordered metal nanohole arrays made by a two-step replication of honeycomb structures of anodic alumina," *Science*, vol. 268(9), pp. 1466-1468, 1995.
- [28] A. I. Vorobjova, B. G. Shulitskii, and E. L. Prudnikova, "Formation of template from anodic aluminum oxide to carbon nanotubes deposition," *Nano- Mikrosist. Tekh.*, vol. 9, pp. 39-43, 2007.
- [29] V. A. Sokol, *Electrochemical Technology for Hybrid Integrated Circuits*, Bestprint, Minsk, 2004.
- [30] S. Esconjauregui, C. Whelan, and K. Maex, "The reasons why metals catalyze the nucleation and growth of carbon nanotubes and other carbon nanomorphologies," *Carbon*, vol. 47, pp. 659-669, 2009.
- [31] S.-H. Jeong, H.-Y. Hwang, S.-K. Hwang, and K.-H. Lee, "Carbon nanotubes based on anodic aluminum oxide nanotemplate," *Carbon*, vol. 42, pp. 2073-2080, 2004.
- [32] X.T. Hoang, D.T. Nguyen, B.C. Dong, and H.N. Nguyen, "Advances in Natural Sciences," *Nanoscience and Nanotechnology*, vol. 4, p. 035013, 5 pages, 2013.
- [33] V. I. Povstugar, A. A. Shakov, S. S. Mikhailova, E. V. Voronina, and E. P. Elsukov, "Decomposition of difficult X-ray photoelectron spectra by means of fast discrete transformation of fourier." *Zh. Anal. Khim.*, vol. 53(8), pp. 795-799, 1998 [*J. Anal. Chem.*, vol. 53(8), pp. 795 (1998)].
- [34] M. M. Brzhezinskaya, E. M. Baitinger, and A. B. Smirnov, "Research of plasmons in the the ion-irradiated single-layer carbon nanotubes by spectroscopic methods," *Fiz. Tverd. Tela*, vol. 48(5), pp. 994-999, 2006 [*Phys. Solid State* 48(5), 994 (2006)].
- [35] A. Mozalev, A. J. Smith, S. Borodin, A. Plihaika, A. W. Hassel, M. Sakairi, and H. akahashi, "Nano-composite anodic films formed from Ta - Al bilayers: structure, formation mechanism and dielectric properties," *Electrochim. Acta*, vol. 54, pp. 935, 2009.
- [36] S. F. Lomaeva, N. V. Ivanov, E. P. Elsukov, and F. Z. Gil'mutdinov, "The temperature stability of Fe₃C in the systems received by mechanoactivation of Fe in liquid organic environments," *Zh. Strukt. Khim.*, vol. 45(Suppl. 1), pp. 160-163, 2004 [*J. Struct. Chem.*, vol. 45(Suppl. 1), pp. S160 (2004)].
- [37] A.S. Basaev, B.G. Shulitskii, A.I. Vorobjova, E.L. Prudnikova, V.A. Labunov, A.M. Mozalev, Yu.P. Shaman, and V.N. Kukin, "Nanocomposite carbon material with ordered structure synthesized using anodic alumina oxide," *Nanotechnol. in Russia*, vol. 6(3-4), pp. 171-180, 2011.
- [38] A.I. Vorobjova and B.G. Shulitskii, "Aligned carbon tubes synthesized using porous aluminum oxide," *Russian Microelectronics*, vol. 41(5), pp. 285-292, 2012.
- [39] I.V. Roslyakov, K.S. Napolskii, P.V. Evdokimov, et al., "Thermal properties of anodic alumina membranes," *Nanosystems: physics, chemistry, mathematics*, vol. 4(1), pp. 120-129, 2013.
- [40] S. Wernick and R. Pinner, *The Surface Treatment and Finishing of Aluminum and Its Alloys*, ASM International, Metals Park, Ohio, United States, 1957; Sudpromgiz, Leningrad, 1960.
- [41] Yu. D. Tret'yakov, *Solid Phase Reactions*, Khimiya, Moscow, 1978.
- [42] A. R. West, *Solid State Chemistry and Its Applications*, Wiley, New York, 1987; Mir, Moscow, 1988.
- [43] L. Fernández Romero, J. M. Montero-Moreno, E. Pellicer, F. Peiró, A. Cornet, J. R. Morante, M. Sarret, and C. Müller, "Assessment of the thermal stability of anodic alumina membranes at high temperatures," *Mater. Chem. Phys.*, vol. 111, pp. 542-547, 2008.
- [44] S.K. Hwang, J. Lee, S.H. Jeong, P.S. Lee, and K.H. Lee, "Fabrication of carbon nanotube emitters in an anodic aluminium oxide nanotemplate on a Si wafer by multi-step anodization," *Nanotechnology*, vol. 16, pp. 850-858, 2005.
- [45] N. S. Xu and H. Ejaz, "Novel cold cathode materials and applications," *Mater. Sci. Eng., R*, vol. 48, pp. 47-189, 2005.
- [46] W. I. Milne, K. B. K. Teo, G. A. J. Amaratunga, P. Legagneux, L. Gangloff, J.P. Schnell, V. Semet, V. T. Binh, and O. Groening, "Carbon nanotubes as field emission sources," *J. Mater. Chem.*, vol. 14, pp. 933-938, 2004.
- [47] H. Orikasa, N. Inokuma, S. Itisanronnachai, X.H. Wang, O. Kitakami, and T. Kyotani, "Template synthesis of water-dispersible and

- magnetically responsive carbon nano test tubes,” *Chem. Commun.* (Cambridge), vol. 19, pp. 2215-2219, 2008.
- [48] H. Gao, X. B. Wu, J. T. Li, G. T. Wu, J. Y. Lin, K. Wu, and D. S. Xu, “Hydrogen adsorption of open tipped insufficiently graphitized multiwalled carbon nanotubes,” *Appl. Phys. Lett.*, vol. 83, pp. 3389-3394, 2003.
- [49] A.I. Vorobjova and B.G. Shulitskii, “Formation of carbon tube arrays on metal electrodes with use of porous aluminum oxide,” *Nano-Mikrosist. Tekh.*, vol. 11, pp. 5-11, 2012.
- [50] A.I. Vorobyeva and E.A. Outkina, “Receiving thin porous oxides of aluminum with the regular ordered structure,” *Russian Microelectronics*, vol. 34(2), pp. 147-156, 2005.
- [51] X.Y. Han and W.Z. Shen, “Improved two-step anodization technique for ordered porous anodic aluminum membranes,” *J. of Electroanalytical Chemistry*, vol. 655, pp. 56-64, 2011.
- [52] A.I. Vorobyeva, E.A. Utkina, and O.V. Komar, “Study of metal pillar nanostructure formation with thin porous alumina template,” *Thin Solid Films*, vol. 548(12), pp. 109-117, 2013.
- [53] B.B. Chesnakov and R.A. Buyanov, “Features of the mechanism of formation of carbon nanofibers with various crystal structure from hydrocarbons on the catalysts containing metals of subgroup of iron,” *Membranes, the Series of critical technologies*, vol. 4(28), pp. 75-79, 2005.
- [54] Z.W. Pan, B.H. Chang, C.Y. Wang, et al., “Very long carbon nanotubes,” *Nature*, vol. 394, pp. 631-632, 1998.
- [55] S.Q. Feng, D.P. Yu, G. Hu, X.F. Zhang, and Z. Zhang, “The HREM observation of cross-sectional structure of carbon nanotubes,” *J. Phys. Chem. Sol.*, vol. 58, pp. 1887-1892, 1997.
- [56] Savas Berber and David Tománek, “Stability differences and conversion mechanism between nanotubes and scrolls,” *Phys. Rev. B*, vol. 69, pp. 233404-1 – 233404-4, 2004.
- [57] A.G. Tkachyov and I.V. Zolotukhin, *Apparatura and methods of synthesis of carbon nanostructures*, M.: Mechanical engineering-1, 2007.
- [58] N.M. Persiantseva, O.V. Popovicheva, A.M. Starik, et al., “About hydrophily of the black particles which are formed in the combustion chamber of the jet engine,” *Letter in J. of Theoretical Fiziks*, vol. 26(18), pp. 50-56, 2000.
- [59] L. A. Apresyan., D.V. Vlasov., T.V. Vlasova., et al., “The reactor with the activated hydrogen for synthesis of carbon nanotubes,” *J. Theoretical Fiziks*, vol. 76(12), pp. 140-142, 2006.
- [60] L. Yang and Rashid Bashir, “Electrical/electrochemical impedance for rapid detection of foodborne pathogenic bacteria,” *Biotechnology Advances*, vol. 26(2), pp. 135-141, 2008.
- [61] F. Lu, L. Gu, M.J. Meziani, et al., “Advances in Bioapplications of Carbon Nanotubes,” *Adv. Mater.*, vol. 21, pp. 139-152, 2009.
- [62] K. Lee, J.H. Kwon, S.L. Moon, et al., “Sensor controls on the basis of carbon nanotubes to define of pH solution,” *Materials Letters*, vol. 14-15, pp. 3201-3203, 2007.
- [63] A. I. Drapeza, et al., “Integrated massifs of capacitor sensors on the basis of nanoporous oxide of aluminum for cultural control methods of microbiological pollution,” International scientific conf. “Medelektronika” - 2008. Minsk, December 11-12, P. 75, 2008.
- [64] S. Krutovertsev, et al., “Sensors of microhumidity of technical gas environments,” *Electronics*, vol. 1, pp. 72, 2008.
- [65] X.B. Wu, J.T. Li, G.T. Wu, et al., “Hydrogen adsorption of open-tipped insufficiently graphitized multiwalled carbon nanotubes,” *Appl. Phys. Lett.*, vol. 83, pp. 3389-3394, 2003.
- [66] Jani Abdul Mutalib Md, D. Losic, and N.H. Voelcker, “Nanoporous anodic aluminium oxide: Advances in surface engineering and emerging applications,” *Progress in Materials Science*, vol. 58(1), pp. 636-704, 2013.
- [67] Sandro Carrara, Sara Ghoreishizadeh, Jacopo Olivo, et al., “Fully integrated biochip platforms for advanced healthcare,” *Sensors (Basel)*, vol. 12(8), pp. 11013-11060, 2012.
- [68] G. Che, B.B. Lakshmi, C.R. Martin, and E.R. Fisher, “Chemical vapor deposition based synthesis of carbon nanotubes and nanofibers using a template method,” *Chem. Mater.*, vol. 10(1), pp. 260-267, 1998.
- [69] T. Altalhi, M. Ginic-Markovic, N. Han, S. Clarke, and D. Losic, “Synthesis of carbon nanotube (CNT) composite membranes,” *Membranes*, vol. 1, pp. 37-47, 2011.
- [70] Y. Lei, W. Cai, and G. Wilde, “Highly ordered nanostructures with tunable size, shape and properties: A new way to surface nanopatterning using ultra-thin alumina masks,” *Progress in Materials Science*, vol. 52(7), pp. 465-539, 2007.
- [71] Y. Chen, F. Meng, M. Li, and J. Liu, “Novel capacitive sensor: Fabrication from carbon nanotube arrays and sensing property characterization,” *Sensors and Actuators B*, vol. 140(4), pp. 396-401, 2009.
- [72] T.T. Xu, F.T. Fisher, L.C. Brinson, and R.S. Ruoff, “Bone-shaped nanomaterials for nanocomposite applications,” *Nano Lett.*, vol. 3(8), pp. 1135-1139, 2003.
- [73] T. Yanagishita, M. Sasaki, K. Nishio, and H. Masuda, “Carbon nanotubes with a triangular cross-section, fabricated using anodic porous alumina template,” *Adv. Mater.*, vol. 16(5), pp. 429-432, 2004.
- [74] S.H. Jeong, H.Y. Hwang, S.K. Hwang, and K.H. Lee, “Carbon nanotubes based on anodic aluminum oxide nano-template,” *Carbon*, vol. 42(10), pp. 2073-2080, 2004.
- [75] H.Y. Jung, J. Kim, J. Hahn, and J.S. Suh, “Well-ordered semiconducting linearly joined carbon nanotube devices at room temperature,” *Chem. Phys. Lett.*, vol. 402(4-6), pp. 535-538, 2005.
- [76] P.L. Chen, J.K. Chang, C.T. Kuo, and F.M. Pan, “Anodic aluminum oxide template assisted growth of vertically aligned carbon nanotube arrays by ECR-CVD,” *Diamond Related Materials*, vol. 13(11-12), pp. 1949-1953, 2004.
- [77] M.J. Kim, T.Y. Lee, J.H. Choi, J.B. Park, J.S. Lee, S.K. Kim, et al., “Growth of carbon nanotubes with anodic aluminum oxide formed on the catalytic metal-coated Si substrate,” *Diamond Related Materials*, vol. 12(3-7), pp. 870-873, 2003.
- [78] H. Chen, A. Roy, Jong-Beom Baek, L. Zhu, J. Qu, and L. Dai, “Controlled growth and modification of vertically-aligned carbon

- nanotubes for multifunctional applications,” *Materials Science and Engineering R*, vol. 70(7), pp. 63-91, 2010.
- [79] M. R. Maschmann, A. D. Franklin, T. D. Sands, and T. S. Fisher, “Optimization of carbon nanotube synthesis from porous anodic Al-Fe-Al templates,” *Carbon*, vol. 45, pp. 2290-2296, 2007.
- [80] M. R. Maschmann, A. D. Franklin, P. B. Amama, D. N. Zakharov, and E. A. Stach, “Vertical single- and double-walled carbon nanotubes grown from modified porous anodic alumina templates,” *Nanotechnology*, vol. 17, pp. 3925-3929, 2006.
- [81] J. Zuidema, X. Ruan, and T. S. Fisher, “Optical properties of ordered carbon nanotube arrays grown in porous anodic alumina templates,” *Optics Express*, vol. 21, pp. 22053-22062, 2013.
- [82] A. Vorobjova, A. Prudnikava, Y. Shaman, B. Shulitski, V. Labunov, and S. Gavrilov, “Specific features of the carbon nanotubes nucleation and growth in the porous alumina membrane,” *Advances in Materials Science and Applications*, vol. 3(2), pp. 46-52, 2014.
- [83] A.I. Vorobjeva, O.M. Komar, S. L. Prischepa, and E.A. Utkina, “Formation and properties of nickel nanopillars in porous oxide of aluminum,” *Nano-microsystems*, vol. 1(1), pp. 15-20, 2014.
- [84] H. Pan, B. Liu, J. Yi, C. Poh, S. Lim, J. Ding, Y. Feng, CHA Huan, and J. Lin, “Growth of singlecrystalline Ni and Co nanowires via electrochemical deposition and their magnetic properties,” *J. Phys. Chem. B*, vol. 109, pp. 3094-3098, 2005.
- [85] C. R. Martin, Nanomaterials: a membrane-based synthetic approach, *Science*, vol. 266, pp. 1961-1966, 1994.
- [86] X. Pan, Z. Fan, W. Chen, Y. Ding, H. Luo, and X. Bao, “Enhanced ethanol production inside carbon-nanotube reactors containing catalytic particles,” *Nature Materials*, vol. 6, pp. 507-511, 2007.
- [87] M. R. Maschmann, P. B. Amam, A. Goyal, Z. Iqbal, and T. S. Fisher, “Freestanding vertically oriented single-walled carbon nanotubes synthesized using microwave plasma-enhanced CVD,” *Carbon*, vol. 44, pp. 2758-2763, 2006.



Research and Innovation in Carbon Nanotube-Based Composites

Edited by Dr. Brahim Attaf

ISBN 978-0-9889190-1-3

Hard cover, 136 pages

Publisher: The World Academic Publishing Co. Ltd.

Published in printed edition: 30, December 2015

Published online: 30, December 2015

This book of nanoscience and nanotechnology provides an overview for researchers, academicians and industrials to learn about scientific and technical advances that will shape the future evolution of composite materials reinforced with carbon nanotubes (CNTs). It involves innovation, addresses new solutions and deals with the integration of CNTs in a variety of high performance applications ranging from engineering and chemistry to medicine and biology. The presented chapters will offer readers an open access to global studies of research and innovation, technology transfer and dissemination of results and will respond effectively to challenges related to this complex and constantly growing subject area.

How to cite this book chapter

Alla Vorobjova, Vladimir Labunov and Boris Shulitski (2015). Carbon Nanotube-Based Composites Synthesized Using Porous Aluminum Oxide, *Research and Innovation in Carbon Nanotube-Based Composites*, Dr. Brahim Attaf (Ed.), ISBN 978-0-9889190-1-3, WAP-AMSA, Available from: <http://www.academicpub.org/amsa/>

World Academic Publishing - Advances in Materials Science and Applications

